UC-406
LBL-26444 c.1

Lawrence Berkeley Laboratory
UNIVERSITY OF CALIFORNIA

Materials & Chemical Sciences Division

RECEIVED
LAWRENCE
BERKELEY LABORATORY

JUL 6 1989

LIBRARY AND
DOCUMENTS SECTION

Presented at the NATO Advanced Study Institute on Superconductivity Electronics, Il Ciocco, Italy, June 26–July 8, 1988, and to be published in the Proceedings

Squid Concepts and Systems

J. Clarke

November 1988

For Reference

Not to be taken from this room

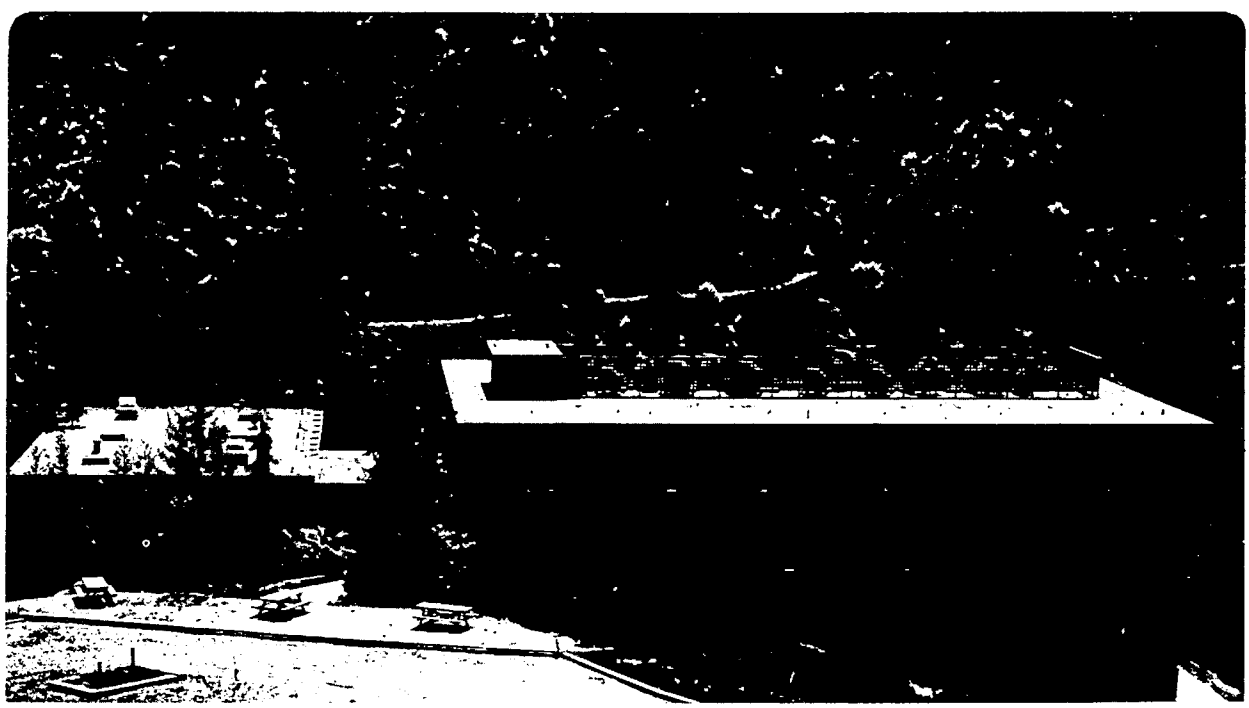

LBL-26444 c.1

Prepared for the U.S. Department of Energy under Contract Number DE-AC03-76SF00098.

DISCLAIMER

This document was prepared as an account of work sponsored by the United States Government. While this document is believed to contain correct information, neither the United States Government nor any agency thereof, nor the Regents of the University of California, nor any of their employees, makes any warranty, express or implied, or assumes any legal responsibility for the accuracy, completeness, or usefulness of any information, apparatus, product, or process disclosed, or represents that its use would not infringe privately owned rights. Reference herein to any specific commercial product, process, or service by its trade name, trademark, manufacturer, or otherwise, does not necessarily constitute or imply its endorsement, recommendation, or favoring by the United States Government or any agency thereof, or the Regents of the University of California. The views and opinions of authors expressed herein do not necessarily state or reflect those of the United States Government or any agency thereof or the Regents of the University of California.

SQUID CONCEPTS AND SYSTEMS

John Clarke

Department of Physics, University of California
and
Materials and Chemical Sciences Division, Lawrence Berkeley Laboratory
1 Cyclotron Road, Berkeley, California 94720

I. INTRODUCTION

Superconducting QUantum Interference Devices (SQUIDs) are the most sensitive detectors of magnetic flux currently available. They are amazingly versatile, being able to measure any physical quantity that can be converted to a flux, for example, magnetic field, magnetic field gradient, current, voltage, displacement, and magnetic susceptibility. As a result, the applications of SQUIDs are wide ranging, from the detection of tiny magnetic fields produced by the human brain and the measurement of fluctuating geomagnetic fields in remote areas to the detection of gravity waves and the observation of spin noise in an ensemble of magnetic nuclei.

SQUIDs combine two physical phenomena, flux quantization, the fact that the flux Φ in a closed superconducting loop is quantized[1] in units of the flux quantum $\Phi_0 \equiv h/2e \cong 2.07 \times 10^{-15}$ Wb, and Josephson tunneling[2]. There are two kinds of SQUIDs. The first[3], the dc SQUID, consists of two Josephson junctions connected in parallel in a superconducting loop, and is so named because it can be operated with a steady current bias. The second[4,5], the rf SQUID, involves a single Josephson junction interrupting the current flow around a superconducting loop, and is operated with a radiofrequency flux bias. In both cases, the output from the SQUID is periodic with period Φ_0 in the magnetic flux applied to the loop. One generally is able to detect an output signal corresponding to a flux change of much less than one flux quantum.

In this chapter I try to give an overview of the current state of the SQUID art. I cannot hope to describe all of the SQUIDs that have been made or, even less, all of the applications in which they have been successfully used. I begin, in Sec. II, with a brief review of the resistively-shunted Josephson junction, with particular emphasis on the effects of noise. Section III contains a description of the dc SQUID: how these devices are made and operated, and the limitations imposed by noise. Section IV contains a similar description of the properties of rf SQUIDs, but because there has been little development of these devices in the 1980's, I shall keep this section relatively brief. In Sec.V, I describe a selection of instruments based on SQUIDs and mention some of their applications. Section VI contains a discussion of the impact of high temperature superconductivity on SQUIDs, and of future prospects in this area, while Sec.VII contains a few concluding remarks.

II. THE RESISTIVELY SHUNTED JUNCTION

A Josephson junction[2] consists of two superconductors separated by a thin insulating barrier. Cooper pairs of electrons (or holes) are able to tunnel through the barrier, maintaining phase coherence in the process. The applied current, I, controls the difference $\delta = \phi_1 - \phi_2$ between the phases of the two superconductors according to the current-phase relation

$$I = I_0 \sin \delta, \tag{2.1}$$

where I_0 is the critical current, that is, the maximum supercurrent the junction can sustain. When the current is increased from zero, initially there is no voltage

across the junction, but for $I > I_0$ a voltage V appears, and δ evolves with time according to the voltage frequency relation

$$\dot{\delta} = 2eV/\hbar = 2\pi V/\Phi_0. \tag{2.2}$$

A high quality Josephson tunnel junction has a hysteretic current-voltage (I - V) characteristic. As the current is increased from zero, the voltage switches abruptly to a nonzero value when I exceeds I_0, but returns to zero only when I is reduced to a value much less than I_0. This hysteresis must be eliminated for SQUIDs operated in the conventional manner, and one does so by shunting the junction with an external shunt resistance. The "resistively shunted junction" (RSJ) model [6,7] is shown in Fig.1(a). The junction has a critical current I_0 and is in parallel with its self-capacitance C and with its shunt resistance R, which has a current noise source $I_N(t)$ associated with it. The equation of motion is

$$C\dot{V} + I_0 \sin\delta + V/R = I + I_N(t). \tag{2.3}$$

Neglecting the noise term for the moment and setting $V = \hbar\dot{\delta}/2e$, we obtain

$$\frac{\hbar C}{2e}\ddot{\delta} + \frac{\hbar}{2eR}\dot{\delta} = I - I_0 \sin\delta = -\frac{2e}{\hbar}\frac{\partial U}{\partial \delta}, \tag{2.4}$$

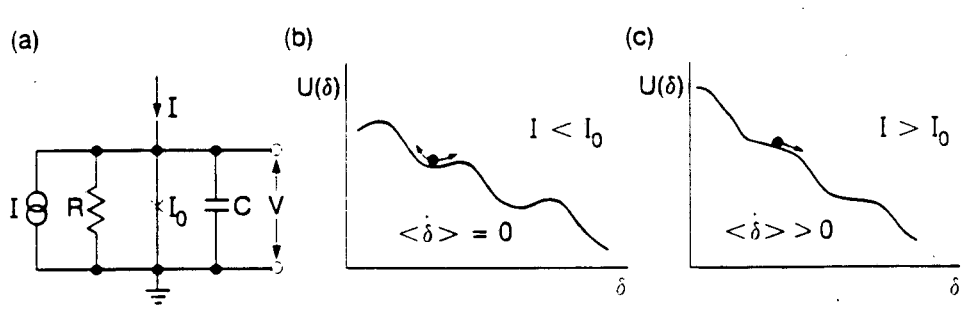

Fig. 1(a) The resistively shunted Josephson junction; (b) and (c) show the tilted washboard model for $I < I_0$ and $I > I_0$.

where

$$U = -\frac{\Phi_0}{2\pi}(I\delta + I_0 \cos\delta). \tag{2.5}$$

One obtains considerable insight into the dynamics of the junction by realizing that Eq. (2.4) also describes the motion of a ball moving on the "tilted washboard" potential U. The term involving C represents the mass of the particle, the 1/R term represents the damping of the motion, and the average "tilt" of the washboard is proportional to -I. For values of $I < I_0$, the particle is confined to one of the potential wells [Fig. 1(b)], where it oscillates back and forth at the plasma frequency[1] $\omega_p = (2\pi I_0/\Phi_0 C)^{1/2}\,[1-(I/I_0)^2]^{1/4}$. In this state $\langle\dot{\delta}\rangle$ and hence the average voltage across the junction are zero (< > represents a time average). When the current is increased to I_0, the tilt increases, and when I exceeds I_0, the particle rolls down the washboard; in this state $\langle\dot{\delta}\rangle$ is nonzero, and a voltage appears across the junction [Fig.1(c)]. As the current is increased further, $\langle\dot{\delta}\rangle$ increases, as does V. For the nonhysteretic case, as soon as I is reduced below I_0 the particle becomes trapped in one of the wells, and V returns to zero. In this, the overdamped case, we require[6,7]

$$\beta_C \equiv (2\pi I_0 R/\Phi_0)RC = \omega_J RC \lesssim 1; \tag{2.6}$$

$\omega_J / 2\pi$ is the Josephson frequency corresponding to the voltage I_0 R.

We introduce the effects of noise by restoring the noise term to Eq. (2.4) to obtain the Langevin equation

$$\frac{\hbar C}{2e}\ddot{\delta} + \frac{\hbar}{2eR}\dot{\delta} + I_0 \sin\delta = I + I_N(t). \tag{2.7}$$

In the thermal noise limit, the spectral density of $I_N(t)$ is given by the Nyquist formula

$$S_I(f) = 4k_B T/R, \tag{2.8}$$

where f is the frequency. It is evident that $I_N(t)$ causes the tilt in the washboard to fluctuate with time. This fluctuation has two effects on the junction. First, when I is less than I_0 , from time to time fluctuations cause the total current $I + I_N(t)$ to exceed I_0 , enabling the particle to roll out of one potential minimum into the

next. For the underdamped junction, this process produces a series of voltage pulses randomly spaced in time. Thus, the time average of the voltage is nonzero even though $I < I_0$, and the I - V characteristic is "noise-rounded" at low voltages.[8] Because this thermal activation process reduces the observed value of the critical current, there is a minimum value of I_0 for which the two sides of the junction remain coupled together. This condition may be written as

$$I_0\Phi_0/2\pi \gtrsim 5k_BT, \tag{2.9}$$

where $I_0\Phi_0 / 2\pi$ is the coupling energy of the junction[2] and the factor of 5 is the result of a computer simulation[9]. For T = 4.2K, we find $I_0 \gtrsim 0.9\mu A$.

The second consequence of thermal fluctuations is voltage noise. In the limit $\beta_C << 1$ and for $I > I_0$, the spectral density of this noise at a measurement frequency f_m that we assume to be much less than the Josephson frequency f_J is given by[10,11]

$$S_V(f_m) = \left[1+\frac{1}{2}\left(\frac{I_0}{I}\right)^2\right]\frac{4k_BTR_D^2}{R} \cdot \left\{\begin{array}{c}\beta_C << 1\\ I > I_0\\ f_m << f_J\end{array}\right\} \tag{2.10}$$

The first term on the right-hand side of Eq. (2.10) represents the Nyquist noise current generated at the measurement frequency f_m flowing through the dynamic resistance $R_d \equiv dV/dI$ to produce a voltage noise - see Fig. 2. The

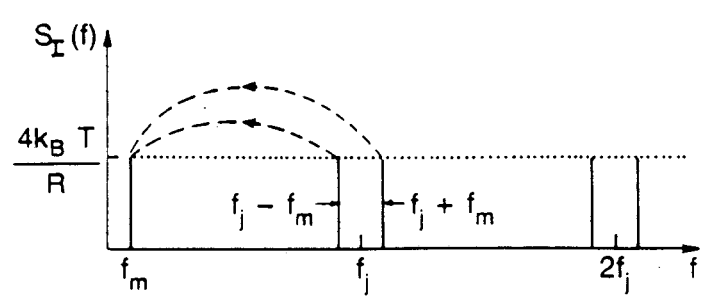

Fig. 2 Schematic representation for the noise terms in Eq.(2.10). The Nyquist noise generated in the resistor at frequency f_m contributes directly at f_m; that generated at $f_J \pm f_m$ is mixed down to f_m .

second term, $(1/2)(I_0 / I)^2 (4k_BT/R)\ R_d^2$, represents Nyquist noise generated at frequencies $f_J \pm f_m$ mixed down to the measurement frequency by the Josephson oscillations and the inherent nonlinearity of the junction. The factor $(1/2)(I_0 / I)^2$ is the mixing coefficient, and it vanishes for sufficiently large bias currents. The mixing coefficients for the Nyquist noise generated near harmonics of the Josephson frequencies, $2f_J$, $3f_J$, ---, are negligible in the limit $f_m / f_J << 1$.

At sufficiently high bias current, the Josephson frequency f_J exceeds k_BT/h, and quantum corrections[12] to Eq. (2.10) become important, provided the term $(1/2)(I_0 / I)^2$ is not too small. The requirement for observing significant quantum corrections is $eI_0R / k_BT >> 1$. The spectral density of the voltage noise becomes

$$S_V(f_m) = \left[\frac{4k_BT}{R} + \frac{2\,e\,V}{R}\left(\frac{I_0}{I}\right)^2 \coth\left(\frac{eV}{k_BT}\right)\right] R_d^2, \quad \left\{\begin{array}{c} \beta_C << 1 \\ I > I_0 \\ f_m << f_J \end{array}\right\} \qquad (2.11)$$

where we have assumed that $hf_m / k_BT << 1$, so that the first term on the right-hand side of Eq. (2.11) remains in the thermal limit. In the limit $T \rightarrow 0$, the second term, $(2eV/R)\ (I_0 / I)^2 R_d^2$, represents noise mixed down from zero point fluctuations near the Josephson frequency.

This concludes our review of the RSJ, and we now turn our attention to the dc SQUID.

III. THE DC SQUID

A. A First Look

The essence of the dc SQUID[3] is shown in Fig. 3(a). Two junctions are connected in parallel on a superconducting loop of inductance L. Each junction is resistively shunted to eliminate hysteresis on the I -V characteristics, which are shown in Fig. 3(b) for $\Phi = n\Phi_0$ and $(n + 1/2)\Phi_0$, where Φ is the external flux applied to the loop and n is an integer. If we bias the SQUID with a constant current ($> 2\ I_0$), the voltage across the SQUID oscillates with period Φ_0 as we steadily increase Φ, as indicated in Fig. 3(c). The SQUID is generally operated on the steep part of the V - Φ curve where the transfer

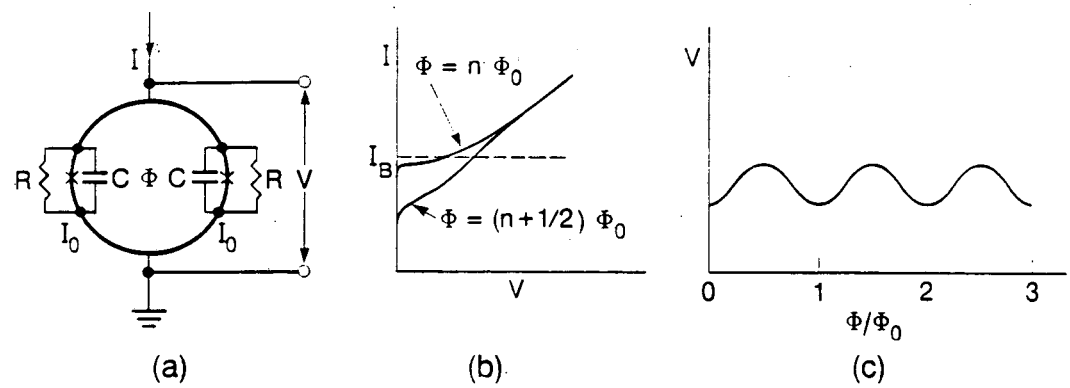

Fig. 3(a) The dc SQUID; (b) I-V characteristics; (c) V vs. Φ/Φ_0 at constant bias current I_B.

coefficient, $V_\Phi \equiv |(\partial V/\partial \Phi)_I|$, is a maximum. Thus, the SQUID produces an output voltage in response to a small input flux $\delta\Phi$ ($<< \Phi_0$), and is effectively a flux-to-voltage transducer.

Before we give a detailed description of the signal and noise properties of the SQUID, it may be helpful to give a simplified description that, although not rigorous, gives some insight into the operation of the device. We assume the two junctions are identical and arranged symmetrically on the loop. We further assume, for simplicity, that the bias current is swept from zero to a value above the critical current of the two junctions at a frequency much higher than $d\Phi/\Phi_0 dt$. In the absence of any applied flux (or with $\Phi = n\,\Phi_0$), there is no current circulating around the loop and the bias current divides equally between the two junctions. The measured critical current is $2I_0$ (if we ignore noise rounding). If we apply a magnetic flux, Φ, the flux in the loop will be quantized and will generate a current $J = -\Phi / L$, where we have neglected the effects of the two junctions [Figs. 4(a) and (b)]. The circulating current adds to the bias current flowing through junction 1 in Fig. 4(a) and subtracts from that flowing through 2. In this naive picture, the critical current of junction 1 is reached when $I/2 + J = I_0$, at which point the current flowing through junction 2 is $I_0 - 2J$. Thus, the SQUID switches to the voltage state when $I = 2I_0 - 2J$. As Φ is increased to $\Phi_0 / 2$, J increases to $\Phi_0 / 2L$ [Fig. 4(b)], and the critical current falls to $2I_0 - \Phi_0 / L$ [Fig. 4(c)]. As the flux is increased beyond $\Phi_0 / 2$, however, the SQUID makes a transition from the flux state n = 0 to n = 1, and J changes sign [Fig. 4(b)]. As we increase Φ to Φ_0, J is reduced to zero and the critical current

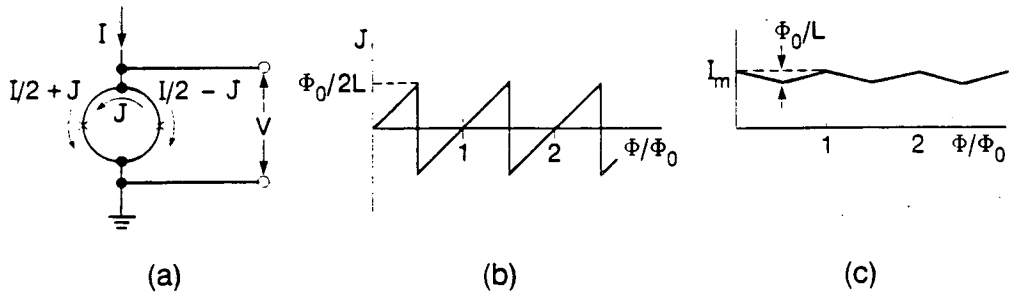

Fig. 4 Simplistic view of the dc SQUID: (a) a magnetic flux Φ generates a circulating current J that is periodic in Φ as shown in (b); as a result (c), the maximum supercurrent I_m is also periodic in Φ.

is restored to its maximum value $I_m = 2I_0$ [Fig. 4(c)]. In this way the critical current oscillates as a function of Φ.

Continuing with our simplified model, we see that the voltage change across the SQUID (at the peak of the current sweep) as we change Φ from 0 to $\Phi_0 / 2$ is $\Delta V = (\Phi_0 / L)R/2$, where R/2 is the parallel resistance of the two shunts. Hence, $V_\Phi = \Delta V / (\Phi_0 / 2) = R / L$.

We also can estimate the equivalent flux noise of the SQUID. If the noise voltage across the SQUID is $V_N(t)$ with a spectral density $S_V(f)$, the corresponding flux noise referred to the SQUID loop is just

$$S_\Phi(f) = S_V(f)/ V_\Phi^2. \tag{3.1}$$

A convenient way of characterizing the flux noise is in terms of the noise energy per unit bandwidth,

$$\varepsilon(f) = S_\Phi(f) / 2L. \tag{3.2}$$

If we assume that the noise in the SQUID is just the Nyquist noise in the shunt resistor with spectral density $4k_BT$ (R/2), we find $\varepsilon(f) = k_BTL/R$. Although these results are not quantitatively correct, they do give the correct scaling with the various parameters. For example, we see that to lower $\varepsilon(f)$ we should reduce T

and L while using the largest possible value of R subject to the I - V characteristic remaining nonhysteretic.

Exact results for the signal and noise can be obtained only from computer simulation. The results show that the plots of the circulating supercurrent and the critical current vs. Φ become smoothed. Furthermore, the noise voltage is higher than Nyquist noise because of mixed-down noise; unfortunately the magnitude of this noise cannot be obtained analytically.

One final remark is appropriate at this point. To observe quantum interference effects, we require the modulation depth of the critical current, Φ_0 / L, to be much greater than the root mean square noise current in the loop, $\langle I_N^2 \rangle^{1/2} = (k_B T / L)^{1/2}$. This condition can be written $L \lesssim \Phi_0^2 / 5k_B T$, where the factor of 1/5 is the result of a computer analysis[9]. For T = 4.2K, we find $L \lesssim 15$ nH.

B. Thermal Noise in the SQUID : Theory

A model for noise calculations is shown in Fig. 5. This figure shows two independent Nyquist noise currents, $I_{N1}(t)$ and $I_{N2}(t)$, associated with the two shunt resistors. The phase differences across the junctions, $\delta_1(t)$ and $\delta_2(t)$, obey the following equations:[13-15]

$$V = \frac{\hbar}{4e}\left(\dot{\delta}_1 + \dot{\delta}_2\right), \tag{3.3}$$

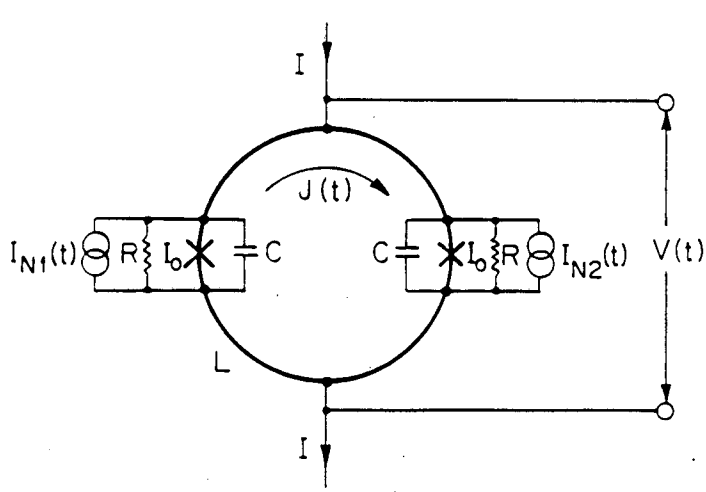

Fig.5 Model of dc SQUID showing noise sources associated with the shunt resistors.

$$J = \frac{\Phi_0}{2\pi L}\left(\delta_1 - \delta_2 - \frac{2\pi\Phi}{\Phi_0}\right), \tag{3.4}$$

$$\frac{\hbar C}{2e}\ddot{\delta}_1 + \frac{\hbar}{2eR}\dot{\delta}_1 = \frac{I}{2} - J - I_0 \sin\delta_1 + I_{N1}, \tag{3.5}$$

and

$$\frac{\hbar C}{2e}\ddot{\delta}_2 + \frac{\hbar}{2eR}\dot{\delta}_2 = \frac{I}{2} + J - I_0 \sin\delta_2 + I_{N2}. \tag{3.6}$$

Equation (3.3) relates the voltage to the average rate of change of phase; Eq. (3.4) relates the current in the loop, J, to $\delta_1 - \delta_2$ and to Φ; and Eqs. (3.5) and (3.6) are Langevin equations coupled via J. These equations have been solved numerically for a limited range of values of the noise parameter $\Gamma = 2\pi k_B T/I_0\Phi_0$, reduced inductance $\beta = 2\,LI_0 / \Phi_0$ and hysteresis parameter β_C. For typical SQUIDs in the ^{4}He temperature range, $\Gamma = 0.05$. One computes the time-averaged voltage V vs. Φ, and hence finds V_Φ, which, for a given value of Φ, peaks smoothly as a function of bias current. The transfer function exhibits a shallow maximum around $(2n + 1)\,\Phi_0 / 4$. One computes the noise voltage for a given value of Φ as a function of I, and finds that the spectral density is white at frequencies much less than the Josephson frequency. For each value of Φ, the noise voltage peaks smoothly at the value of I where V_Φ is a maximum. From these simulations, one finds that the noise energy has a minimum when $\beta \approx 1$. For $\beta = 1$, $\Gamma = 0.05$, $\Phi = (2n + 1)\,\Phi_0 / 4$ and for the value of I at which V_Φ is a maximum, the results can be summarized as follows:

$$V_\Phi \approx R/L, \tag{3.7}$$

$$S_V(f) \approx 16 k_B T R, \tag{3.8}$$

and

$$\varepsilon(f) \approx 9 k_B T L/R. \tag{3.9}$$

We see that our rough estimate of V_Φ in Sec. IIIA was rather accurate, but that the assumption that the noise spectral density was given by the Nyquist result underestimated the computed value by a factor of about 8.

It is often convenient to eliminate R from Eq. (3.9) using the expression $R = (\beta_C \Phi_0 / 2\pi I_0 C)^{1/2}$. We find

$$\varepsilon(f) \approx 16\, k_B T (LC/\beta_C)^{1/2}. \quad (\beta_C \lesssim 1) \tag{3.10}$$

Equation (3.10) gives a clear prescription for improving the resolution: one should reduce T, L and C. A large number of SQUIDs with a wide range of parameters have been tested and found to have white noise energies generally in good agreement with the predicted values. It is common practice to quote the noise energy of SQUIDs in units of $\hbar$ ($\approx 10^{-34}$J sec = 10^{-34}JHz^{-1}).

In closing this discussion, we emphasize that although $\varepsilon(f)$ is a useful parameter for characterizing the resolution of SQUIDs with different inductances, it is not a complete specification because it does not account fully for the effects of current noise in the SQUID loop. We defer a discussion of this point to Sec. V.D.

C. Practical dc SQUIDs

Modern dc SQUIDs are invariably made from thin films with the aid of either photolithography or electron beam lithography. A major concern in the design is the need to couple an input coil inductively to the SQUID with rather high efficiency. This problem was elegantly solved by Ketchen and Jaycox,[16,17] who introduced the idea of depositing a spiral input coil on a SQUID in a square washer configuration. The coil is separated from the SQUID with an insulating layer. The version[18] of this design made at UC Berkeley is shown in Fig. 6. These devices are made in batches of 36 on 50mm diameter oxidized silicon wafers in the following way. First, a 30nm thick Au (25 wt % Cu) film is deposited and patterned to form the resistive shunts. Next, we sputter a 100nm thick Nb film and etch it to form the SQUID loop and a strip that eventually contacts the inner end of the spiral coil. The third film is a 200 nm SiO layer with 2 μm diameter windows for the junctions, a larger window to give access to the CuAu shunt, and a window at each end of the Nb strip to provide connections to the spiral coil. The next step is to deposit and lift off the 300 nm thick Nb spiral coil, which has 4, 20 or 50 turns. At this point, we usually dice the wafer into

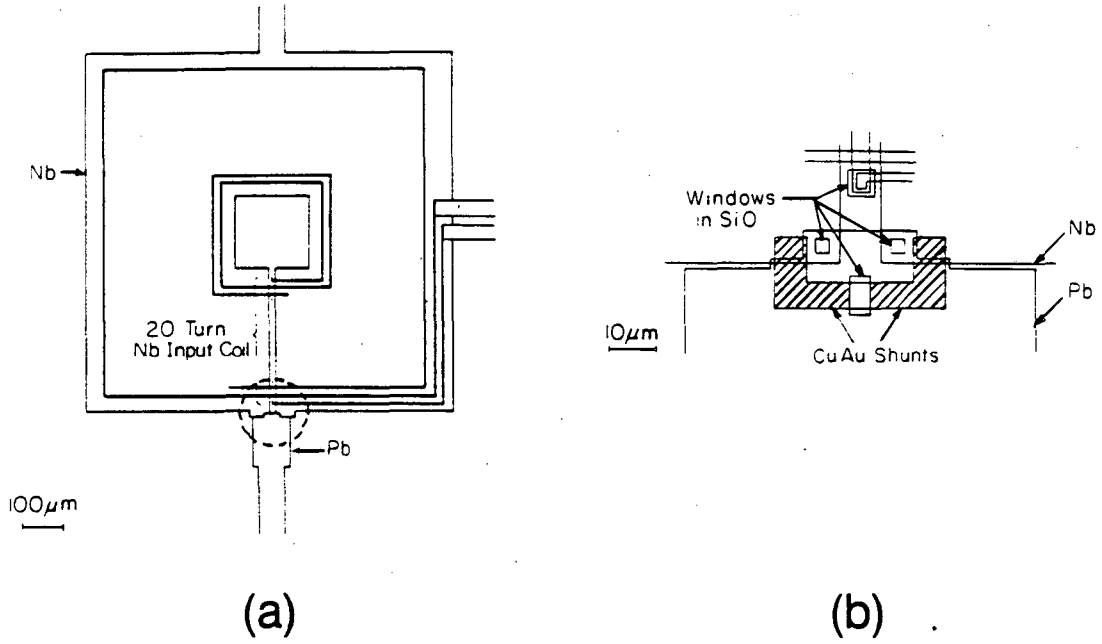

Fig.6 (a) Configuration of planar dc SQUID with overlaid spiral input coil; (b) expanded view of junctions and shunts.

chips, each with a single SQUID which is completed individually. The device is ion milled to clean the exposed areas of Nb and CuAu. We have two procedures for forming the oxide barrier. In one, we oxidize the Nb in a rf discharge in Ar containing 5 vol % O_2, and deposit the 300 nm Pb (5wt % In) counterelectrode which completes the junctions and makes contact with the shunts. In the other process, we deposit approximately 6 nm of Al and form Al_2O_3 by exposing[19] it to O_2. A photograph of the completed SQUID and a scanning electron micrograph of the junctions is shown in Fig. 7. The shunt resistance R is typically 8 Ω, and the estimated capacitance C about 0.5 pF.

Jaycox and Ketchen[17] showed that a square washer (with no slit) with inner and outer edges d and w has an inductance L (loop) = $1.25\mu_0 d$ in the limit w >> d. They gave the following expressions for the inductances of the SQUID, L, and of the spiral coil, L_i, and for the mutual inductance, M_i, and coupling coefficient, α^2, between the spiral coil and the SQUID:

$$L = L\,(\text{loop}) + L_j, \tag{3.11}$$

$$L_i = n^2\,(L - L_j) + L_s, \tag{3.12}$$

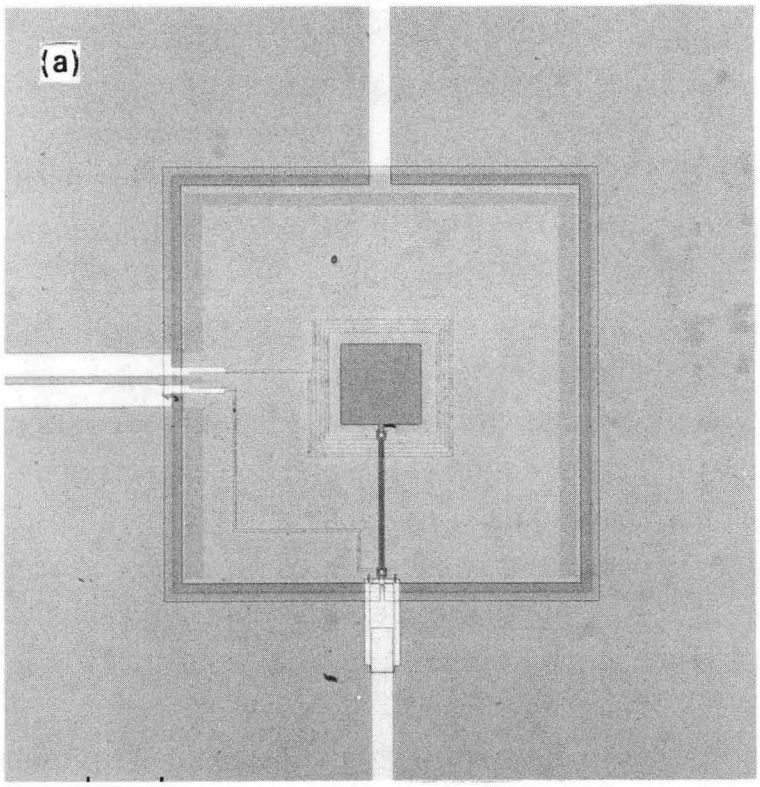

CBB 883-1734

(b)

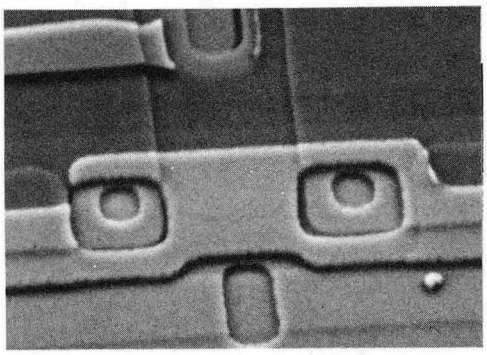

XBB 850-9959

Fig.7(a) Photograph of planar dc SQUID made at UC Berkeley, with 4-turn input coil; the square washer is about 1mm across. (b) Electron micrograph of junctions prior to deposition of counterelectrode; each junction is about 3μm across.

$$M_i = n(L-L_j) \tag{3.13}$$

and

$$\alpha^2 = (1-L_J/L)/\ [1+L_s n^2(L-L_j)]. \tag{3.14}$$

Here, L_j is the parasitic inductance associated with the junctions, n is the number of turns of the input coil and L_s is the stripline inductance of this coil. For the SQUID just described with a 50-turn input coil, one measures $L_i \approx 800$ nH, $M_i \approx 16$ nH and $\alpha^2 \approx 0.75$. These results are in good agreement with the predictions of the above expressions if one takes the predicted value L(loop) ≈ 0.31 nH and assumes $L_j \approx 0.09$ nH to give $L \approx 0.4$ nH. The stripline inductance (~10 nH) is insignificant for a 50-turn coil.

References 20-25 are a selection of papers describing SQUIDs fabricated on the basis of the Ketchen-Jaycox design. Some of the devices involve edge junctions in which the counterelectrode is a strip making a tunneling contact to the base electrode only at the edge. This technique enables one to make junctions with a small area and thus a small self-capacitance without resorting to electron-beam lithography. However, stray capacitances are often critically important. As has been emphasized by a number of authors, parasitic capacitance between the square washer and the input coil can produce resonances that, in turn, induce structure on the I-V characteristics and give rise to excess noise. One way to reduce these effects is to lower the shunt resistance in order to increase the damping. A different approach is to couple the SQUID to the signal via an intermediary superconducting transformer[24], so that the number of turns on the SQUID washer and the parasitic capacitance are reduced. Knuutila et al.[25] successfully damped the resonances in the input coil by terminating the stripline with a matched resistor. An alternate coupling scheme has been adopted by Carelli and Foglietti[26], who fabricated thin-film SQUIDs with many loops in parallel. The loops are coupled to a thin-film input coil surrounding them.

D. Flux-locked Loop

In most, although not all, practical applications one uses the SQUID in a feedback circuit as a null detector of magnetic flux[27]. One applies a modulating flux to the SQUID with a peak-to-peak amplitude $\Phi_0/2$ and a frequency f_m usually between 100 and 500 kHz, as indicated in Fig. 8. If the quasistatic flux in the SQUID is exactly $n\Phi_0$ the resulting voltage is a rectified version of the input signal, that is, it contains only the frequency $2f_m$ [Fig. 8(a)]. If this voltage is sent through a lock-in detector referenced to the fundamental frequency f_m, the output will be zero. On the other hand, if the quasistatic flux is $(n + 1/4)\Phi_0$, the voltage across the SQUID is at frequency f_m [Fig. 8(b)], and the output from the lock-in will be a maximum. Thus, as one increases the flux from $n\Phi_0$ to $(n + 1/4)\Phi_0$, the output from the lock-in will increase steadily; if one reduces the flux from $n\Phi_0$ to $(n - 1/4)\Phi_0$, the output will increase in the negative direction [Fig. 8(c)].

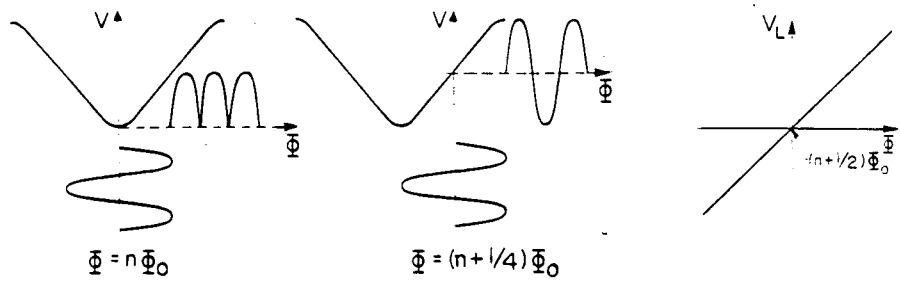

Fig. 8 Flux modulation scheme showing voltage across the SQUID for (a) $\Phi = n\Phi_0$ and (b) $\Phi = (n+1/4)\Phi_0$. The output V_L from the lock-in detector vs. Φ is shown in (c).

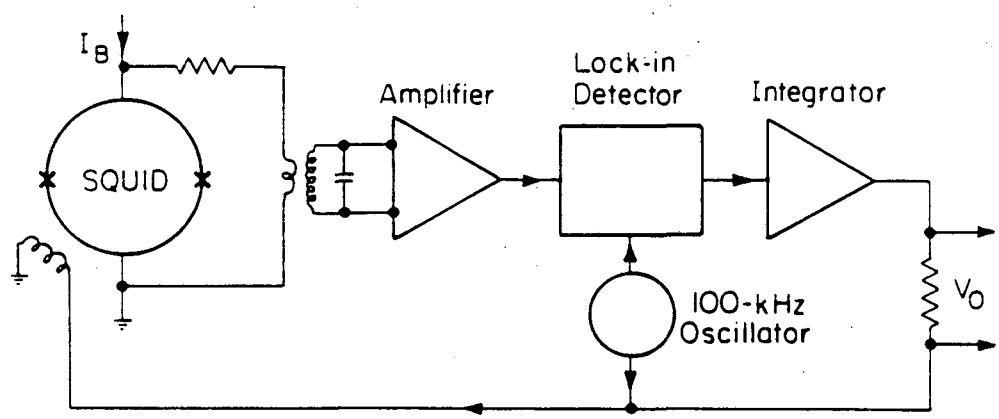

Fig. 9 Modulation and feedback circuit for the dc SQUID.

The alternating voltage across the SQUID is coupled to a low-noise preamplifier, usually at room temperature, via either a cooled transformer[28] or a cooled LC series-resonant circuit[27]. The first presents an impedance N^2R_d to the preamplifier, and the second, an impedance Q^2R_d, where R_d is the dynamic resistance of the SQUID at the bias point, N is the turns ratio of the transformer, and Q is the quality factor of the tank circuit. The value of N or Q is chosen to optimize the noise temperature of the preamplifier; with careful design, the noise from the amplifier can be appreciably less than that from the SQUID at 4.2 K.

Figure 9 shows a typical flux-locked loop in which the SQUID is coupled to the preamplifier via a cooled transformer. An oscillator applies a modulating flux to the SQUID. After amplification, the signal from the SQUID is lock-in detected and sent through an integrating circuit. The smoothed output is connected to the modulation and feedback coil via a large series resistor R_f. Thus, if one applies a flux $\delta\Phi$ to the SQUID, the feedback circuit will generate an

opposing flux - $\delta\Phi$, and a voltage proportional to $\delta\Phi$ appears across R_f. This technique enables one to measure changes in flux ranging from much less than a single flux quantum to many flux quanta. The use of a modulating flux eliminates 1/f noise and drift in the bias current and preamplifier. Using a modulation frequency of 500 kHz, a double transformer between the SQUID and the preamplifier, and a two-pole integrator, Wellstood et al.[18] achieved a dynamic range of $\pm 2 \times 10^7$ $Hz^{1/2}$ for signal frequencies up to 6 kHz, a frequency response from 0 to 70 kHz (±3 dB), and a maximum slew rate of 3×10^6 Φ_0 sec^{-1}.

E. Thermal Noise in the dc SQUID : Experiment

One determines the spectral density of the equivalent flux noise in the SQUID by connecting a spectrum analyzer to the output of the flux-locked loop. A representative power spectrum[29] is shown in Fig. 10: above a 1/f noise region, the noise is white at frequencies up to the roll-off of the feedback circuit. In this particular example, with L = 200pH and R = 8Ω, the measured flux noise was $S_\Phi^{1/2} = (1.9 \pm 0.1) \times 10^{-6}\Phi_0 Hz^{-1/2}$, in reasonable agreement with the predictions of Eqs. (3.7) and (3.8). The corresponding flux-noise energy was 4×10^{-32} $JHz^{-1} \approx 400\ \hbar$. Many groups have achieved noise energies that are comparable or, with lower values of L or C, somewhat better.

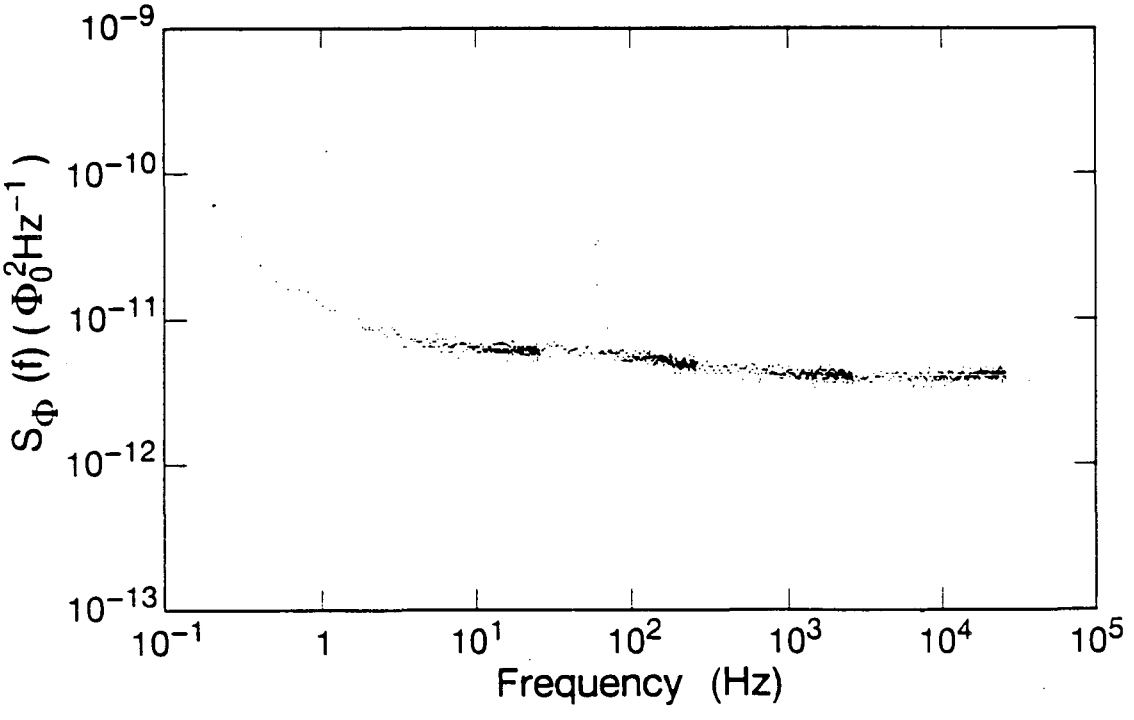

Fig.10 Spectral density of equivalent flux noise for dc SQUID with a Pb body : L = 0.2nH, R = 8Ω, and T = 4.2K (courtesy F.C. Wellstood).

Rather recently, Wellstood et al.[30] have operated SQUIDs in a dilution refrigerator at temperatures T below 1K , using a second dc SQUID as a preamplifier. They found that the noise energy scaled accurately with T at temperatures down to about 150 mK, below which the noise energy became nearly constant. This saturation was traced to heating in the resistive shunts, which prevented them from cooling much below 150mK. This heating is actually a hot-electron effect:[31,32] the bottleneck in the cooling process is the rate at which the electrons can transfer energy to the phonons which, in turn, transfer energy to the substrate. The temperature of the shunts was lowered by connecting each of them to a CuAu "cooling fin" of large volume. The hot electrons diffuse into the fins where they rapidly transfer energy to other electrons. Since the "reaction volume" is now greatly increased, the numbers of electrons and phonons interacting are also increased, and the electron gas is cooled more effectively. In this way, the effective electron temperature was reduced to about 50mK when the SQUID was at a bath temperature of 20mK, with a concomitant reduction in ε to about $5\hbar$. Very recently Ketchen et al.[33] have achieved a noise energy of about $2\hbar$ at 0.3 K in a SQUID with L = 100 pH and C = 0.14 pF.

F. 1/f Noise in dc SQUIDs

The white noise in dc SQUIDs is well understood. However, some applications of SQUIDs, for example neuromagnetism, require good resolution at frequencies down to 0.1 Hz or less, and the level of the 1/f or "flicker" noise becomes very important.

There are at least two separate sources of 1/f noise in the dc SQUID[34]. The first arises from 1/f fluctuations in the critical current of the Josephson junctions, and the mechanism for this process is reasonably well understood[35]. In the process of tunneling through the barrier, an electron becomes trapped on a defect in the barrier and is subsequently released. While the trap is occupied, there is a local change in the height of the tunnel barrier and hence in the critical current density of that region. As a result, the presence of a single trap causes the critical current of the junction to switch randomly back and forth between two values, producing a random telegraph signal. If the mean time between pulses is τ, the spectral density of this process is a Lorentzian,

$$S(f) \propto \frac{\tau}{1+(2\pi f\tau)^2}, \tag{3.15}$$

namely white at low frequencies and falling off as $1/f^2$ at frequencies above $1/2\pi\tau$. In many cases, the trapping process is thermally activated, and τ is of the form

$$\tau = \tau_0 \exp (E/k_0T), \tag{3.16}$$

where τ_0 is a constant and E is the barrier height.

In general, there may be several traps in the junction, each with its own characteristic time τ_i. One can superimpose the trapping processes, assuming them to be statistically independent, to obtain a spectral density[36]

$$S(f) \propto \int dE\, D(E)\left[\frac{\tau_0 \exp(E/k_BT)}{1+(2\pi f\tau_0)^2 \exp(2E/k_BT)}\right], \tag{3.17}$$

where D(E) is the distribution of activation energies. The term in square brackets is a strongly peaked function of E, centered at $\tilde{E} \equiv k_BT\ln(1/2\pi f\tau_0)$, with a width ~ k_BT. Thus, at a given temperature, only traps with energies within a range k_BT of $\tilde{E}$ contribute significantly to the noise. If one now assumes D(E) is broad with respect to k_BT, one can take $D(\tilde{E})$ outside the integral, and carry out the integral to obtain

$$S(f,T) \propto \frac{k_BT}{f} D(\tilde{E}). \tag{3.18}$$

In fact, one obtains a 1/f-like spectrum from just a few traps.

The magnitude of the 1/f noise in the critical current depends strongly on the quality of the junction as measured by the current leakage at voltages below $(\Delta_1 + \Delta_2)/e$, where Δ_1 and Δ_2 are the energy gaps of the two superconductors. Traps in the barrier enable electrons to tunnel in this voltage range, a process producing both leakage current and 1/f noise. Thus, for a given technology, junctions with low subgap leakage currents will have low 1/f noise. Figure 11 shows an example of a Nb-Al_2O_3-Nb junction with a single trap[37]. The junction was resistively shunted and voltage biased at typically 1.5 μV; the noise currents were measured with a SQUID. At 4.2 K [Fig.11(a)], the noise is approximately Lorentzian; the switching process producing the noise is shown in the inset. Figure 11(b) shows that at 1.5 K the noise is substantially reduced as the trap freezes out. By measuring the temperature dependence of the random telegraph signal, Savo et al.[37] found that τ obeyed Eq. (3.16) with τ_0 = 10 s and

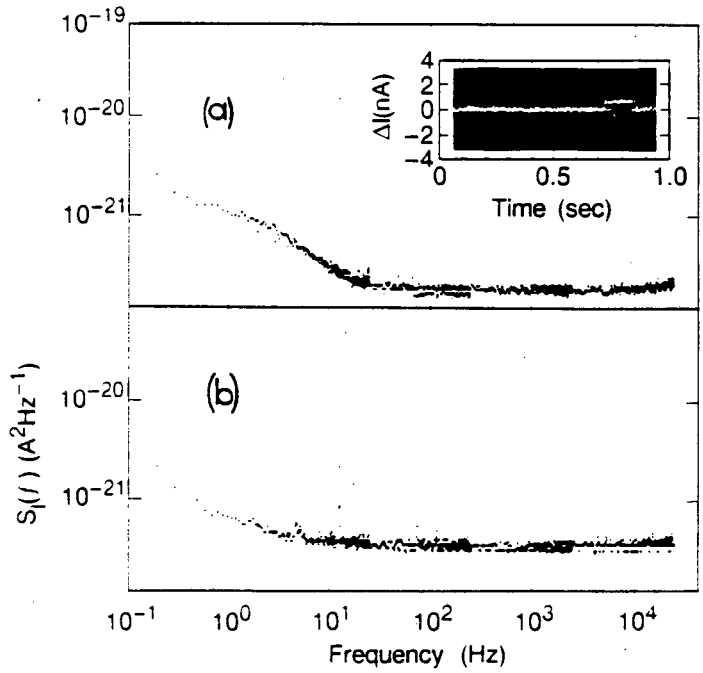

Fig.11 Spectral density of fluctuations in the critical current of a single Nb-Al_2O_3-Nb tunnel junction at (a) 4.2K and (b) 1.5K. Inset in (a) shows fluctuations vs. time (from ref.37).

E = 1.8 meV. Furthermore, τ was exponentially distributed, as expected, with an average value of 107 ms at 4.2 K.

The second source of l/f noise in SQUIDs appears to arise from the motion of flux lines trapped in the body of the SQUID[34], and is less well understood than the critical current noise. This mechanism manifests itself as a flux noise; for all practical purposes the noise source behaves as if an external flux noise were applied to the SQUID. Thus, the spectral density of the l/f flux noise scales as V_Φ^2, and, in particular, vanishes at $\Phi = (n \pm 1/2)\Phi_0$ where $V_\Phi = 0$. By contrast, critical current noise is still present when $V_\Phi = 0$, although its magnitude does depend on the applied flux.

The level of l/f flux noise appears to depend strongly on the microstructure of the thin films. For example, SQUIDs fabricated at Berkeley with Nb loops sputtered under a particular set of conditions show l/f flux noise levels of typically[34] $10^{-10}\ \Phi_0^2\,Hz^{-1}$ at 1 Hz. On the other hand, SQUIDs with Pb loops in exactly the same geometry exhibit a l/f noise level of about $2\times10^{-12}\ \Phi_0^2 Hz^{-1}$ at 1 Hz, arising from critical current fluctuations. Tesche et al.[38]

reported a 1/f noise level in Nb-based SQUIDs of about $3\times10^{-13}\,\Phi_0^2\,Hz^{-1}$, while Foglietti et al.[39] found a critical current 1/f noise corresponding to $2\times10^{-12}\,\Phi_0^2\,Hz^{-1}$, also in Nb based devices. Thus, we conclude that the quality of the Nb films plays a significant role in the level of 1/f flux noise. It is of considerable fundamental and practical interest to understand the mechanism in detail.

There is an important practical difference between the two sources of 1/f noise: critical current noise can be reduced by a suitable modulation scheme, whereas flux noise cannot. To understand how to reduce critical current 1/f noise, we first note that at constant current bias the spectral density of the 1/f voltage noise across the SQUID can be written in the approximate form

$$S_V(f) \approx \frac{1}{2}\left[(\partial V/\partial I_0)^2+L^2V_\Phi^2\right] S_{I_0}(f). \tag{3.19}$$

In Eq. (3.19), we have assumed that each junction has the same level of critical current noise, with a spectral density $S_{I_0}(f)$. The first term on the right is the "in-phase mode", in which each of the two junctions produces a fluctuation of the same polarity. This noise is eliminated (ideally) by the conventional flux modulation scheme described in Sec. III D, provided the modulation frequency is much higher than the 1/f noise frequency. The second term on the right of Eq. (3.19) is the "out-of phase" mode in which the two fluctuations are of opposite polarity and, roughly speaking, result in a current around the SQUID loop. This term appears, therefore, as a flux noise, vanishing for $V_\Phi = 0$, but is not reduced by the usual flux modulation scheme. Fortunately, there are schemes by which this second term, as well as the first, can be reduced.

One such scheme was described by Koch et al.[34] and is also available on the dc SQUID manufactured by BTi[40]. An alternate scheme, second harmonic detection (SHAD), has recently been developed by Foglietti et al.[39], and we shall briefly describe it. In Fig. 12(a) we see that both I and Φ are switched among the three states A: $(+I, \Phi+\Phi_0/4)$, B: $(0, \Phi+\Phi_0/2)$ and C: $(-I,\Phi+3\Phi_0/4)$. If the static flux is $n\Phi_0$ [dashed curve and pulses in Fig.12(a)], the positive and negative voltage pulses across the SQUID are of equal magnitude, and if one detects this signal at twice the modulation frequency, the output is zero. If we apply an additional flux $\delta\Phi$, however, the V-Φ curve is shifted along the Φ-axis [solid curve and pulses in Fig.12(a)], and the pulse heights become unequal. Lock-in detection at twice the modulation frequency produces an output proportional to $\delta\Phi$. The output from the lock-in detector is integrated and fedback to flux-lock

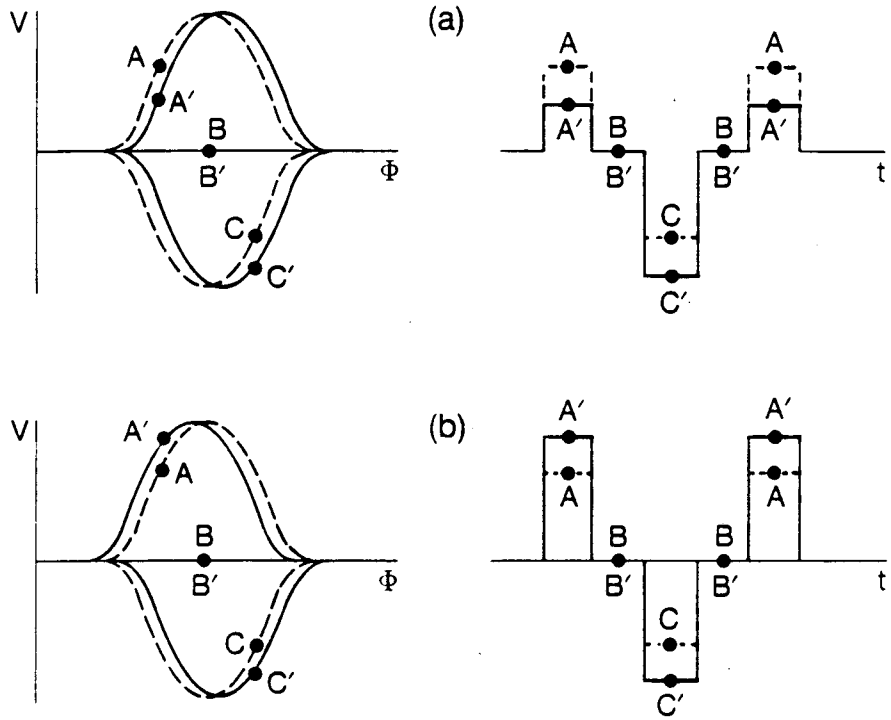

Fig.12 SHAD modulation scheme for a dc SQUID to reduce 1/f noise due to critical current fluctuations: (a) shows the response to an external flux $\delta\Phi$, and (b) the response to a critical current fluctuation (re-drawn from ref. 39).

the SQUID in the usual way. We note that in-phase fluctuations in critical current increase or decrease the magnitude of the voltage across the SQUID, but do not shift the V-Φ curve along the Φ axis. The magnitudes of the voltage pulses grow or shrink in a symmetric way, and still contain no second harmonic component. Thus, the in-phase fluctuations in critical current produce no response. Similarly, the out-of-phase fluctuations produce no response, as we see in Fig. 12(b). These fluctuations produce an effective flux in the SQUID, with a polarity that depends on the direction of I. Thus, the V-Φ curve shifts to the left for positive bias currents and to the right for negative bias currents. The resulting voltage pulses shrink in a symmetric way, producing no component at the second harmonic of the modulation frequency. Finally, we emphasize that any 1/f flux noise produces an output from the lock-in detector in precisely the same way as the applied flux in Fig. 12(a).

Figure 13 shows an example of the reduction in 1/f noise achieved by Foglietti et al.[34] Figure 13(a) shows the noise as measured with a rf SQUID, and Fig. 13(b), with the conventional flux modulation scheme. The reduction in 1/f noise indicates that in-phase critical current fluctuations have been removed.

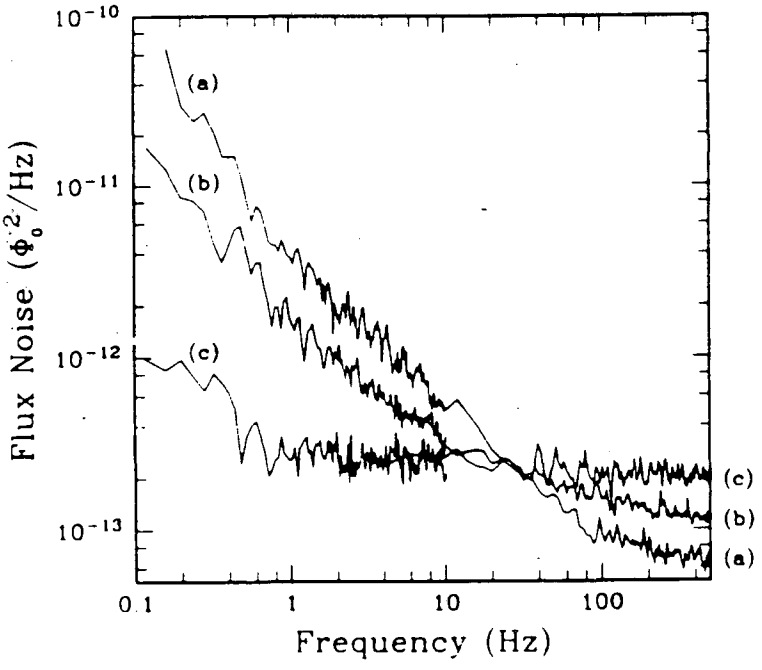

Fig.13 Flux noise spectral density for dc SQUID measured (a) with an rf SQUID small-signal readout scheme, (b) with the flux modulation scheme of Figs.8 and 9 and (c) with SHAD (Fig.12) (re-drawn from ref. 39).

Figure 13(c) shows the considerable reduction in the l/f noise resulting from SHAD: the measured l/f noise was $10^{-12}\,\Phi_0^2 Hz^{-1}$ at 0.1 Hz. We note that SHAD increases the spectral density of the white noise by a factor of 2: V_Φ^2 is reduced by a factor of 4, while the noise is measured only during the 50% of the modulation cycle in which the SQUID is biased.

For measurements at low frequencies, it is clearly advantageous to use a l/f noise reduction scheme for SQUIDs in which the l/f noise is dominated by critical current fluctuations. As stressed repeatedly, however, nothing can be done to reduce l/f flux noise. As we shall see in Sec. VI, l/f flux noise is a particularly serious problem for high-T_C SQUIDs.

G. Alternate Read-Out Schemes

Although the flux modulation method described in Sec. III.D has been used successfully for many years, alternate schemes recently have been developed. These efforts have been motivated, at least in part, by the need to simplify the electronics required for the multichannel systems used in neuromagnetism - see Sec. V.A. Fujimaki and co-workers[41] and Drung and co-workers[42] have devised schemes in which the output from the SQUID is sensed digitally and fed back as

an analog signal to the SQUID to flux-lock the loop. Fujimaki et al.[41] used Josephson digital circuitry to integrate their feedback system on the same chip as the SQUID so that the flux-locked signal was available directly from the cryostat. The system of Drung and co-workers, however, is currently the more sensitive, with a flux resolution of about $10^{-6}\ \Phi_0 Hz^{-1/2}$ in a 50 pH SQUID. These workers also were able to reduce the 1/f noise in the system using a modified version of the modulation scheme of Foglietti et al.[39] Although they need further development, cryogenic digital feedback schemes offer several advantages: they are compact, produce a digitized output for transmission to room temperature, offer wide flux-locked bandwidths, and need not add any noise to the intrinsic noise of the SQUID.

In yet another system, Mück and Heiden[43] have operated a dc SQUID with hysteretic junctions in a relaxation oscillator. The oscillation frequency depends on the flux in the SQUID, reaching a maximum at $(n+1/2)\Phi_0$ and a minimum at $n\Phi_0$. A typical frequency modulation is 100 kHz at an operating frequency of 10 MHz. This technique produces large voltages across the SQUID so that no matching network to the room temperature electronics is required. The room temperature electronics is simple and compact, and the resolution at 4.2 K is about $10^{-5}\Phi_0 Hz^{-1/2}$ with an inductance estimated to be about 80 pH.

IV. THE RF SQUID

A. Principles of Operation

Although the rf SQUID is still the more widely used device because of its long-standing commercial availability, it has seen very little development in recent years. For this reason I will give a rather brief account of its principles and noise limitations, following rather closely descriptions in earlier reviews.[44,45]

The rf SQUID[4,5] shown in Fig.14 consists of a superconducting loop of inductance L interrupted by a single Josephson junction with critical current I_0 and a nonhysteretic current-voltage characteristic. Flux quantization[1] imposes the constraint

$$\delta + 2\pi\Phi_T/\Phi_0 = 2\pi n \qquad (4.1)$$

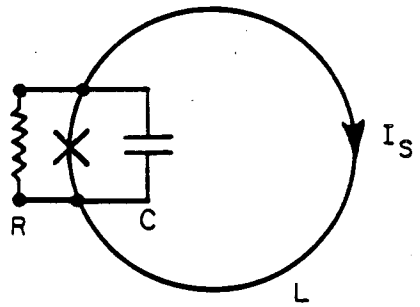

Fig.14 The rf SQUID.

on the total flux Φ_T threading the loop. The phase difference δ across the junction determines the supercurrent

$$I_s = -I_0 \sin (2\pi\Phi_T/\Phi_0) \tag{4.2}$$

flowing in the ring. A quasistatic external flux Φ thus gives rise to a total flux

$$\Phi_T = \Phi - LI_0 \sin (2\pi\Phi/\Phi_0). \tag{4.3}$$

The variation of Φ_T with Φ is sketched in Fig.15(a) for the typical value $LI_0 = 1.25\ \Phi_0$. The regions with positive slope are stable, whereas those with negative slope are not. A "linearized" version of Fig.15(a) showing the path traced out by Φ and Φ_T is shown in Fig.15(b). Suppose we slowly increase Φ from zero. The total flux Φ_T increases less rapidly than Φ because the response flux $-LI_S$ opposes Φ. When I_S reaches I_0, at an applied flux Φ_C and a total flux Φ_{TC}, the junction switches momentarily into a nonzero voltage state and the SQUID jumps from the k = 0 to the k = 1 quantum state. If we subsequently reduce Φ from a value just above Φ_C, the SQUID remains in the k = 1 state until $\Phi = \Phi_0 - \Phi_C$, at which point I_S again exceeds the critical current and the SQUID returns to the k = 0 state. In the same way, if we lower Φ to below $-\Phi_C$ and then increase it, a second hysteresis loop will be traced. We note that this hysteresis occurs provided $LI_0 > \Phi_0/2\pi$; most practical SQUIDs are operated in this regime. For $LI_0 \approx \Phi_0$, the energy ΔE dissipated when one takes the flux around a single hysteresis loop is its area divided by L:

$$\Delta E \approx I_0\Phi_0. \tag{4.4}$$

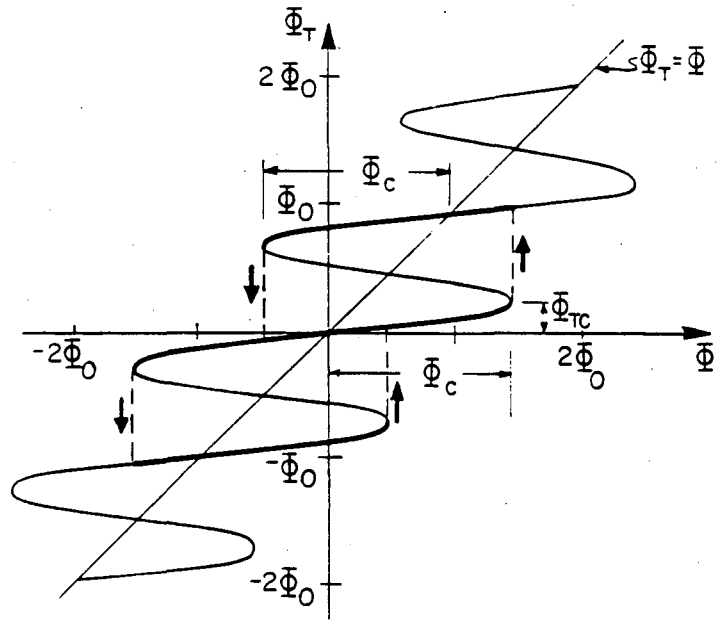

(a)

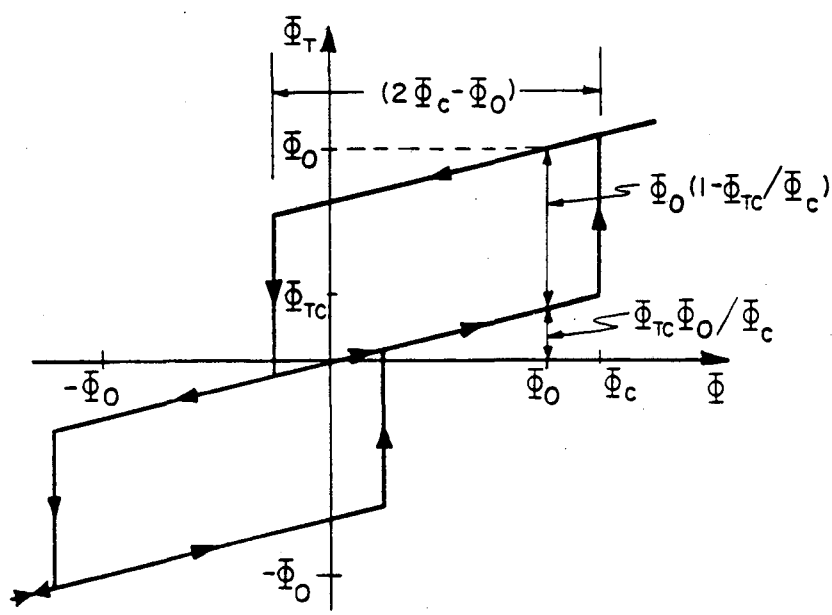

(b)

Fig.15 The rf SQUID: (a) total flux Φ_T vs. Φ for $LI_0 = 1.25\ \Phi_0$; (b) values of Φ_T as Φ is quasistatically increased and then decreased.

We now consider the radio frequency (rf) operation of the device. The SQUID is inductively coupled to the coil of an LC-resonant circuit with a quality factor $Q = R_T/\omega_{rf}L_T$ via a mutual inductance $M = K(LL_T)^{1/2}$ - see Fig. 16. Here,

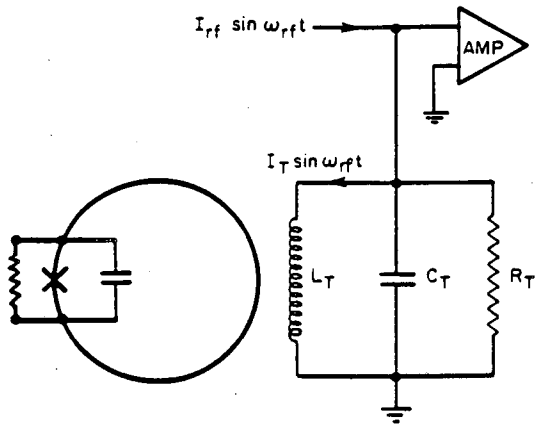

Fig.16 The rf SQUID inductively coupled to a resonant tank circuit.

L_T, C_T, and R_T are the inductance, capacitance and (effective) parallel resistance of the tank circuit, and $\omega_{rf}/2\pi$ is its resonant frequency, typically 20 or 30 MHz. The tank circuit is excited at its resonant frequency by a current I_{rf} sin$\omega_{rf}t$, which generates a current of amplitude $I_T = QI_{rf}$ in the inductor. The voltage V_T across the tank circuit is amplified with a preamplifier having a high input impedance. First, consider the case $\Phi = 0$. As we increase I_{rf} from zero, the peak rf flux applied to the loop is $MI_T = QMI_{rf}$, and V_T increases linearly with I_{rf}. The peak flux becomes equal to Φ_C when $I_T = \Phi_C/M$ or $I_{rf} = \Phi_C/MQ$, at A in Fig.17. The corresponding peak rf voltage across the tank circuit is

$$V_T^{(n)} = \omega_{rf}L_T\Phi_C/M, \tag{4.5}$$

where the superscript (n) indicates $\Phi = n\Phi_0$, in this case with n=0. At this point the SQUID makes a transition to <u>either</u> the k = +1 state or the k = -1 state. As the SQUID traverses the hysteresis loop, energy ΔE is extracted from the tank circuit. Because of this loss, the peak flux on the next half cycle is less than Φ_C, and no transition occurs. The tank circuit takes many cycles to recover sufficient energy to induce a further transition, which may be into either the k = +1 or -1 states. If we now increase I_{rf}, transitions are induced at the same values of I_T and V_T but, because energy is supplied at a higher rate, the stored energy builds up more rapidly after each energy loss ΔE, and transitions occur more frequently. In the absence of thermal fluctuations (Sec. IV.B), the "step" AB in Fig.17 is at constant voltage. At B, a transition is induced on each positive and negative rf

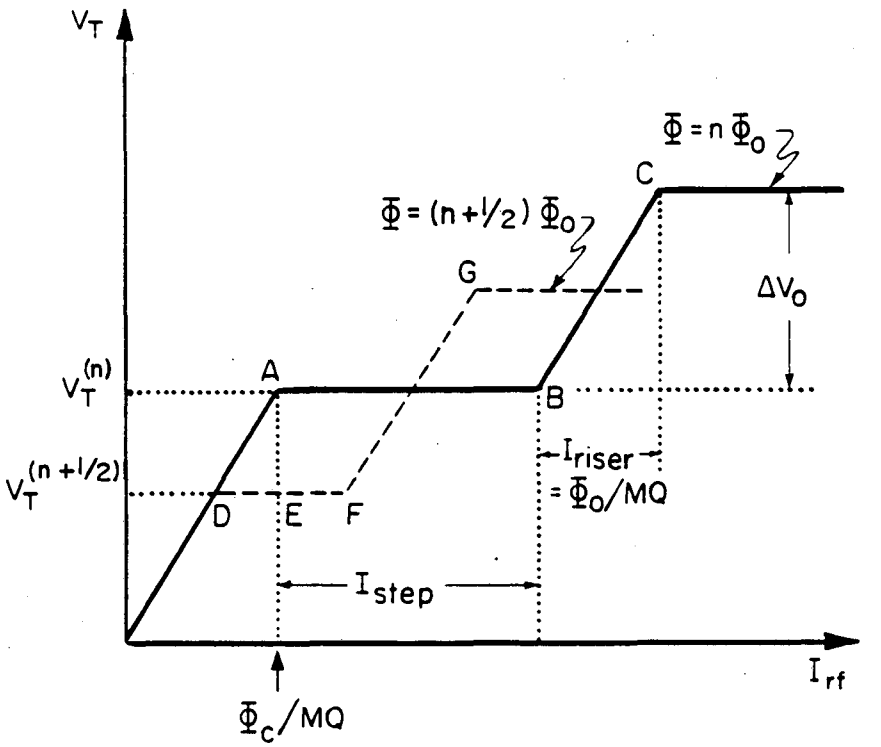

Fig.17 V_T vs. I_{rf} in the absence of thermal noise for $\Phi = n\Phi_0$, $(n+1/2)\Phi_0$.

peak, and a further increase in I_{rf} produces the "riser" BC. At C, transitions from the $k = \pm 1$ to the $k = \pm 2$ states occur, and a second step begins. As we continue to increase I_{rf}, we observe a series of steps and risers.

If we now apply an external flux $\Phi = \Phi_0/2$, the hysteresis loops in Fig.15(b) are shifted by $\Phi_0/2$. Thus, a transition occurs on the positive peak of the rf cycle at a flux $(\Phi_c - \Phi_0/2)$, whereas on the negative peak the required flux is $-(\Phi_c + \Phi_0/2)$. As a result, as we increase I_{rf} from zero, we observe the first step at D in Fig.17 at

$$V_T^{(n+1/2)} = \omega_{rf} L_T (\Phi_C - \Phi_0/2)/M. \tag{4.6}$$

As we increase I_{rf} from D to F, the SQUID traverses only one hysteresis loop, corresponding to the $k = 0$ to $k = +1$ transition at $(\Phi_c - \Phi_0/2)$. A further increase in I_{rf} produces the riser FG, and at G, transitions begin at a peak rf flux $-(\Phi_C + \Phi_0/2)$. In this way, we observe a series of steps and risers for $\Phi = \Phi_0/2$, interlocking those for $\Phi = 0$ (Fig.17). As we increase Φ from zero, the voltage at

which the first step appears will drop to a minimum (D) at $\Phi_0/2$ and rise to its maximum value (A) at $\Phi = \Phi_0$. The change in V_T as we increase Φ from 0 to $\Phi_0/2$, found by subtracting Eq. (4.6) from Eq.(4.5), is $\omega_{rf}L_T\Phi_0/2M$. Thus, for a small change in flux near $\Phi = \Phi_0/4$ we find the transfer function

$$V_\Phi = \omega_{rf}L_T/M. \tag{4.7}$$

At first sight, Eq.(4.7) suggests that we can make V_Φ arbitrarily large by reducing K sufficiently. However, we obviously cannot make K so small that the SQUID has no influence on the tank circuit, and we need to establish a lower bound on K. To operate the SQUID, we must be able to choose a value of I_{rf} that intercepts the first step for all values of Φ : this requirement is satisfied if the point F in Fig. 17 lies to the right of E, that is, if DF exceeds DE. We can calculate DF by noting that the power dissipation in the SQUID is zero at D and $\Delta E(\omega_{rf}/2\pi) \approx I_0\Phi_0\omega_{rf}/2\pi$ at F. Thus, $(I_{rf}^{(F)}-I_{rf}^{(D)})V_T^{(n+1/2)}/2 = I_0\Phi_0\omega_{rf}/2\pi$ (I_{rf} and V_T are peak, rather than rms values). Furthermore, we easily can see that $I_{rf}^{(E)} - I_{rf}^{(D)} = \Phi_0/2MQ$. Assuming $LI_0 \approx \Phi_0$ and using Eq.(4.5), we find that the requirement $I_{rf}^{(E)} > I_{rf}^{(D)}$ can be written in the form

$$K^2Q \gtrsim \pi/4. \tag{4.8}$$

If we set $K \approx Q^{-1/2}$, Eq.(4.7) becomes

$$V_\Phi \approx \omega_{rf}(QL_T/L)^{1/2}. \tag{4.9}$$

To operate the SQUID, one adjusts I_{rf} so that the SQUID remains biased on the first step - see Fig.17 - for all values of Φ. The rf voltage across the tank circuit is amplified and demodulated to produce a signal that is periodic in Φ. A modulating flux, typically at 100kHz and with a peak-to-peak amplitude of $\Phi_0/2$, also is applied to the SQUID, just as in the case of the dc SQUID. The voltage produced by this modulation is lock-in detected, integrated, and fed back as a current into the modulation coil to flux-lock the SQUID.

B. Theory of Noise in the rf SQUID

A detailed theory has been developed for noise in the rf SQUID;[46-54] in contrast to the case for the dc SQUID, noise contributions from the tank circuit and preamplifier also are important. We begin by discussing the intrinsic noise

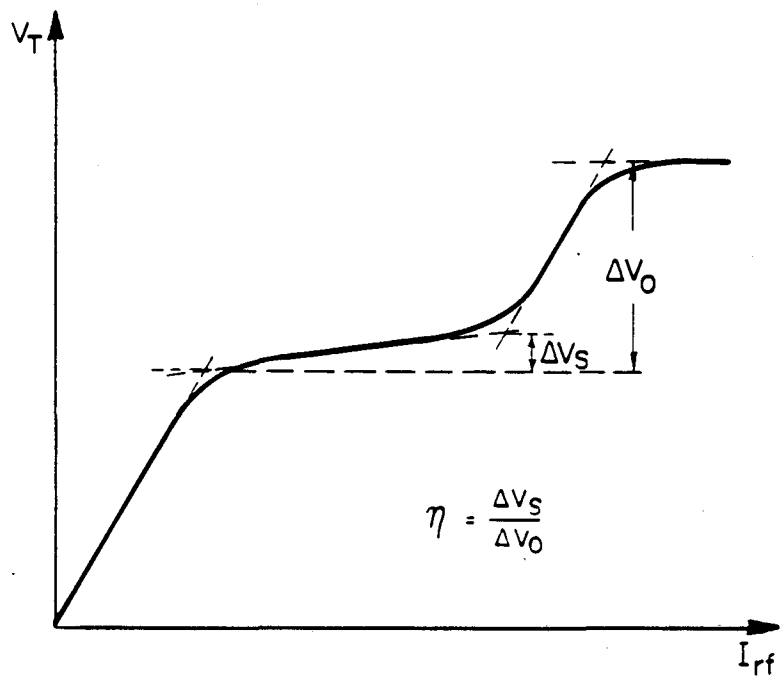

Fig.18 V_T vs. I_{rf} showing the effects of thermal noise.

in the SQUID. In the previous section we assumed that transitions from the k = 0 to the k = 1 state occurred precisely at $\Phi = \Phi_C$. In fact, thermal activation causes the transition to occur stochastically, at lower values of flux. Kurkijärvi[46] calculated the distribution of values of Φ at which the transitions occur; experimental results[55] are in good agreement with his predictions. When the SQUID is driven with an rf flux, the fluctuations in the value of flux at which transitions occur have two consequences. First, noise is introduced on the peak voltage V_T, giving an equivalent intrinsic flux noise spectral density[47,51]

$$S_\Phi^{(i)} \approx \frac{(LI_0)^2}{\omega_{rf}}\left(\frac{2\pi k_B T}{I_0 \Phi_0}\right)^{4/3}. \tag{4.10}$$

Second, the noise causes the steps to tilt (Fig.18), as we easily can see by considering the case for $\Phi = 0$. In the presence of thermal fluctuations the transition from the k = 0 to the k = 1 state (for example) has a certain probability of occurring at any given value of the total flux $\Phi + \Phi_{rf}$. Just to the right of A in Fig.17 this transition occurs at the peak of the rf flux once in many rf cycles. Thus, the probability of the transition occurring in any one cycle is small. On the

other hand, at B a transition must occur at each positive and negative peak of the rf flux, with unity probability. To increase the transition probability, the peak value of the rf flux and hence V_T must increase as I_{rf} is increased from A to B. Jackel and Buhrman[48], introduced the slope parameter η defined in Fig.18, and showed that it was related to $S_\Phi^{(i)}$ by the relation

$$\eta^2 \approx S_\Phi^{(i)} \omega_{rf} / \pi \Phi_0^2, \tag{4.11}$$

provided η was not too large. This relation is verified experimentally.

The noise temperature T_a of typical rf amplifiers operated at room temperature is substantially higher than that of amplifiers operated at a few hundred kilohertz, and is therefore not negligible for rf SQUIDs operated at liquid ^{4}He temperatures. Furthermore, part of the coaxial line connecting the tank circuit to the preamplifier is at room temperature. Since the capacitances of the line and the amplifier are a substantial fraction of the capacitance of the tank circuit, part of the resistance damping the tank circuit is well above the bath temperature. As a result, there is an additional contribution to the noise which we combine with the preamplifier noise to produce an effective noise temperature T_a^{eff}. The noise energy contributed by these extrinsic sources can be shown to be[48,52] $2\pi\eta k_B T_a^{eff}/\omega_{rf}$. Combining this contribution with the intrinsic noise, one finds

$$\varepsilon \approx \frac{1}{\omega_{rf}} \left(\frac{\pi \eta^2 \Phi_0^2}{2L} + 2\pi\eta k_B T_a^{eff} \right). \tag{4.12}$$

Equation (4.12) shows that ε scales as $1/\omega_{rf}$, but one should bear in mind that T_a tends to increase with ω_{rf}. Nonetheless, improvements in performance have been achieved by operating the SQUID at frequencies[56,57] much higher than the usual 20 or 30 MHz. One also can reduce the T_a^{eff} by cooling the preamplifier,[56,58] thereby reducing T_a and reducing the temperature of the tank circuit to that of the bath. However, the best noise energies achieved for the rf SQUID are substantially higher[59] than those routinely obtained with thin-film dc SQUIDs, and for this reason workers requiring the highest possible resolution almost invariably use the latter device.

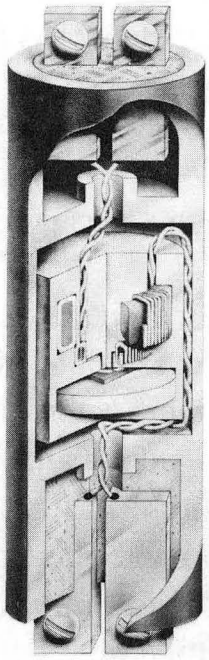

XBB 889-9417

Fig.19 Cut-away drawing of toroidal SQUID (courtesy BTi, inc.).

C. Practical rf SQUIDs

Although less sensitive than the dc SQUID, the rf SQUID is entirely adequate for a wide range of applications. It is therefore more widely used than the dc SQUID, for the simple reason that reliable, easy-to-operate devices have been commercially available since the early 1970's, notably from BTi (formerly SHE). We therefore shall confine ourselves to a brief description of the device available from this company.

Figure 19 shows a cut-away drawing of the BTi rf SQUID[40], which has a toroidal configuration machined from Nb. One way to understand this geometry is to imagine rotating the SQUID in Fig.14 through 360° about a line running through the junction from top to bottom of the page. This procedure produces a toroidal cavity connected at its center by the junction. If one places a toroidal coil in this cavity, a current in the coil produces a flux that is tightly coupled to the SQUID. In Fig.19, there are actually two such cavities, one containing the tank circuit-modulation-feedback coil and the other the input coil. This separation eliminates cross-talk between the two coils. Leads to the two coils are brought out via screw-terminals. The junction is made from thin films of Nb. This device is self-shielding against external magnetic field fluctuations, and has

proven to be reliable and convenient to use. In particular, the Nb input terminals enable one to connect different input circuits in a straightforward way. A typical device has a white noise energy of 5×10^{-29} JHz^{-1}, with a 1/f noise energy of perhaps 10^{-28} JHz^{-1} at 0.1 Hz.

V. SQUID-BASED INSTRUMENTS

Both dc and rf SQUIDs are used as sensors in a far-ranging assortment of instruments. I here briefly discuss some of them: my selection is far from exhaustive, but does include the more commonly used instruments.

Each instrument involves a circuit attached to the input coil of the SQUID. We should recognize from the outset that, in general, the presence of the input circuit influences both the signal and noise properties of the SQUID while the SQUID, in turn, reflects a complex impedance into the input. Because the SQUID is a nonlinear device a full description of the interactions is complicated, and we shall not go into the details here. However, one aspect of this interaction, first pointed out by Zimmerman[60], is easy to understand. Suppose we connect a superconducting pick-up loop of inductance L_P to the input coil of inductance L_i to form a magnetometer, as shown in Fig.20(a). It is easy to show that the SQUID inductance L is reduced to the value

$$L' = L[1-\alpha^2 L_i/(L_i+L_P)], \tag{5.1}$$

where α^2 is the coupling coefficient between L and L_i. We have neglected any stray inductance in the leads connecting L_i and L_P, and any stray capacitance. The reduction in L tends to increase the transfer coefficient of both the dc SQUID [Eq.(3.7)] and the rf SQUID [Eq.(4.9)]. In most cases, the reduction of L and the change in the noise properties will be detectable, but they will not have a major effect on the results presented here.

A. Magnetometers and Gradiometers

One of the simplest instruments is the magnetometer [Fig.20(a)]. A pick-up loop is connected across the input coil to make a superconducting flux transformer. The SQUID and input coil are generally enclosed in a superconducting shield. If one applies a magnetic flux, $\delta\Phi^{(p)}$, to the pick-up loop, flux quantization requires that

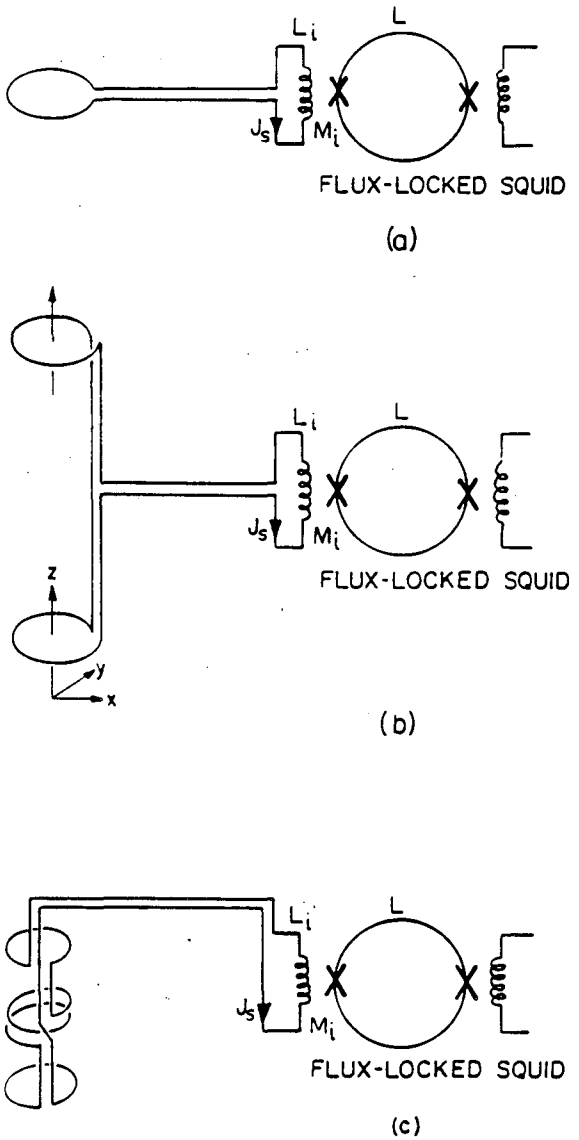

Fig.20 Superconducting flux transformers:(a) magnetometer, (b) first-derivative gradiometer, (c) second-derivative gradiometer.

$$\delta\Phi^{(p)} + (L_i + L_p)J_S = 0, \tag{5.2}$$

where J_S is the supercurrent induced in the transformer. We have neglected the effects of the SQUID on the input circuit. The flux coupled into the SQUID, which we assume to be in a flux-locked loop, is $\delta\Phi = M_i|J_S| = M_i\delta\Phi^{(p)}/(L_i + L_P)$. We find the minimum detectable value of $\delta\Phi^{(p)}$ by equating $\delta\Phi$ with the equivalent flux noise of the SQUID. Defining $S_\Phi^{(p)}$ as the spectral density of the equivalent flux noise referred to the pick-up loop, we find

$$S_\Phi^{(p)} = \frac{(L_p+L_i)^2}{M_i^2} S_\Phi. \tag{5.3}$$

Introducing the equivalent noise energy referred to the pick-up loop, we obtain

$$\frac{S_\Phi^{(p)}}{2L_p} = \frac{(L_p+L_i)^2}{L_i\, L_p} \frac{S_\Phi}{2\alpha^2 L} . \tag{5.4}$$

We observe that Eq.(5.4) has the minimum value

$$S_\Phi^{(p)}/2L_p = 4\varepsilon(f)/\alpha^2 \tag{5.5}$$

when $L_i = L_p$. Thus, a fraction $\alpha^2/4$ of the energy in the pick-up loop is transferred to the SQUID. In this derivation we have neglected noise currents in the input circuit arising from noise in the SQUID, the fact the the input circuit reduces the SQUID inductance, and any possible coupling between the feedback coil of the SQUID and the input circuit.

Having obtained the flux resolution for $L_i = L_p$, we can immediately write down the corresponding magnetic field resolution $B_N^{(p)} = (S_\Phi^{(p)})^{1/2}/\pi r_p^2$, where r_p is the radius of the pick-up loop:

$$B_N^{(p)} = 2\sqrt{2} L_p^{1/2} \varepsilon^{1/2}/\pi r_p^2 \alpha . \tag{5.6}$$

For a loop made from wire of radius r_0, one finds[61] $L_p = \mu_0 r_p[\ln(8r_p/r_0) - 2]$, where $\mu_0 = 4\pi \times 10^{-7}$ henries/meter; for a reasonable range of values of r_p/r_0 we can set $L_P \approx 5\mu_0 r_p$. Thus, we obtain $B_N^{(p)} \approx 2(\mu_0\varepsilon)^{1/2}/\alpha r_P^{3/2}$. This indicates that one can, in principle, improve the magnetic field resolution indefinitely by increasing r_P, keeping $L_i = L_p$. Of course, in practice, the size of the cryostat will impose an upper limit on r_P. If we take $\varepsilon = 10^{-28}$ JHz^{-1} (a somewhat conservative value for an rf SQUID), $\alpha = 1$, and $r_P = 25$ mm, we find $B_N^{(p)} \approx 5 \times 10^{-15}$ tesla Hz$^{-1/2}$ = 5×10^{-11} gauss Hz$^{-1/2}$. This is a much higher sensitivity than that achieved by any nonsuperconducting magnetometer.

Magnetometers have usually involved flux transformers made of Nb wire. For example, one can make the rf SQUID in Fig.19 into a magnetometer merely by connecting a loop of Nb wire to its input terminals. In the case of the thin-film

dc SQUID, one can make an integrated magnetometer by fabricating a Nb loop across the spiral input coil. In this way, Wellstood et al.[18] achieved a magnetic field white noise of 5×10^{-15} tesla $Hz^{-1/2}$ using a pick-up loop with a diameter of a few millimeters.

Magnetometers with typical sensitivities of 0.01 pT $Hz^{-1/2}$ have been used in geophysics in a variety of applications,[62] for example, magnetotellurics, active electromagnetic sounding, piezomagnetism, tectonomagnetism, and the location of hydrofractures. Although SQUID-based magnetometers are substantially more sensitive than any other type, the need to replenish the liquid helium in the field has restricted the extent of their applications. For this reason, the advent of high-temperature superconductors may have considerable impact on this field - see Sec.VI.

An important variation of the flux transformer is the gradiometer. Figure 20(b) shows an axial gradiometer that measures $\partial B_z/\partial z$. The two pick-up loops are wound in opposition and balanced so that a uniform field B_z links zero net flux to the transformer. A gradient $\partial B_z/\partial z$, on the other hand, does induce a net flux and thus generates an output from the flux-locked SQUID. Figure 20(c) shows a second-order gradiometer that measures $\partial^2 B_z/\partial z^2$; Fig.21(a) is a photograph of a practical version.

Thin-film gradiometers based on dc SQUIDs were made as long ago[28] as 1978, and a variety of devices[25,63-67] have been reported since then. To my knowledge, all of the thin film gradiometers made to date have been planar, and therefore measure an off-diagonal gradient, for example, $\partial B_z/\partial x$ or $\partial^2 B_z/\partial x \partial y$. A representative device is shown in Fig.21(b)-(d).

The most important application of the gradiometer thus far is in neuromagnetism[68], notably to detect weak magnetic signals emanating from the human brain. The gradiometer discriminates strongly against distant noise sources, which have a small gradient, in favor of locally generated signals. One can thus use a second-order gradiometer in an unshielded environment, although the present trend is toward using first-order gradiometers in a shielded room of aluminum and mu-metal that greatly attenuates the ambient magnetic noise. In this application, axial gradiometers of the type shown in Fig.20(a) actually sense magnetic field, rather than the gradient, because the distance from the signal source to the pick-up loop is less than the baseline of the gradiometer. The magnetic field sensitivity referred to one pick-up loop is typically 10 fT $Hz^{-1/2}$. Although great progress in this field has been made in recent years, it is generally

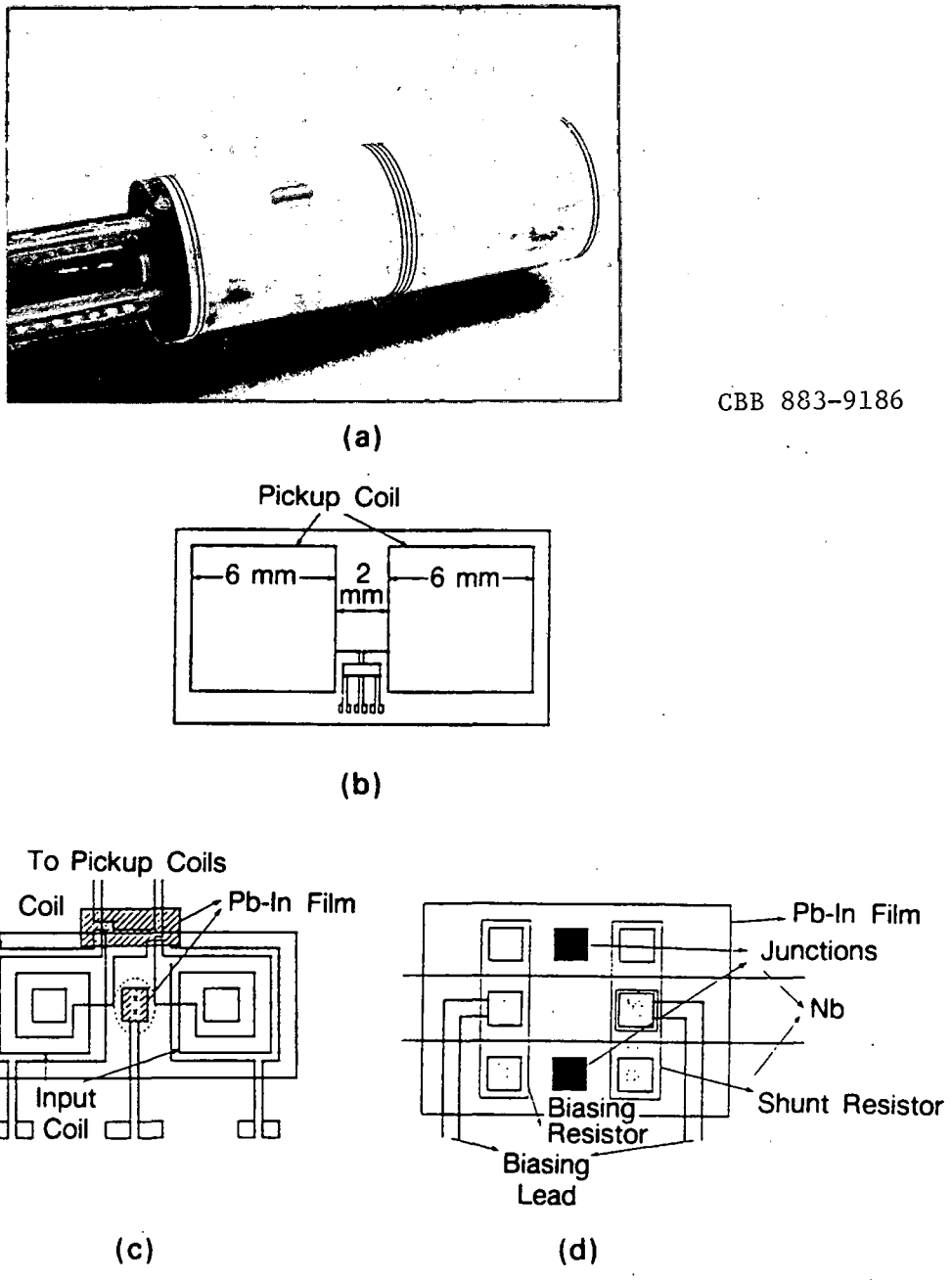

Fig.21 (a) Photograph of wire-wound second-derivative gradiometer for biomedical applications (courtesy BTi, inc.); thin-film first-derivative gradiometer: (b) pick-up loops, (c) two-hole SQUID with spiral input coils, and (d) expanded view of the dotted circle in (c) showing junctions and resistive shunts (from ref. 66).

agreed that one needs an array of 50 to 100 gradiometers to make a clinically viable system. This requirement has greatly spurred the development of

integrated, thin-film devices. For example, Knuutila[69] has reported that a 24-channel first-derivative array is under construction.

There are two basic kinds of measurements made on the human brain. In the first, one detects spontaneous activity: a classic example is the generation of magnetic pulses by subjects suffering from focal epilepsy[70]. The second kind involves evoked response: for example, Romani et al.[71] detected the magnetic signal from the auditory cortex generated by tones of different frequencies. Romani has given a extensive review of this work elsewhere in these proceedings.

There are several other applications of gradiometers. One kind of magnetic monopole detector[72] consists of a gradiometer: the passage of a monopole would link a flux h/e in the pick-up loop and produce a step-function response from the SQUID. Gradiometers have recently been of interest in studies of corrosion and in the location of fractures in pipelines and other structures.

B. Susceptometers

In principle, one easily can use the first-derivative gradiometer of Fig.20(b) to measure magnetic susceptibility χ. One establishes a static field along the z-axis and lowers the sample into one of the pick-up loops. Provided χ is nonzero, the sample introduces an additional flux into the pick-up loop and generates an output from the flux-locked SQUID. A very sophisticated susceptometer is available commercially[73]. Room temperature access enables one to cycle samples rapidly, and one can measure χ as a function of temperature between 1.8 K and 400 K in fields up to 5.5 tesla. The system is capable of resolving a change in magnetic moment as small as 10^{-8} emu.

Novel miniature susceptometers have been developed by Ketchen and co-workers[33,74,75]. One version is shown schematically in Fig.22. The SQUID loop incorporates two pick-up loops wound in the opposite sense and connected in series. The two square pick-up loops, 17.5 μm on a side and with an inductance of about 30 pH, are deposited over a hole in the ground plane that minimizes the inductance of the rest of the device. The SQUID is flux biased at the maximum of V_Φ by means of a control current I_C in one of the pick-up loops. One can apply a magnetic field to the two loops by means of the current I_F; by passing a fraction of this current into the center tap I_C, one can achieve a high degree of electronic balance between the two loops. The sample to be studied is placed over one of the loops, and the output from the SQUID when the field is applied is directly proportional to the magnetization. At 4.2 K, the susceptometer is capable of detecting the magnetization due to as few as 3000 electron spins.

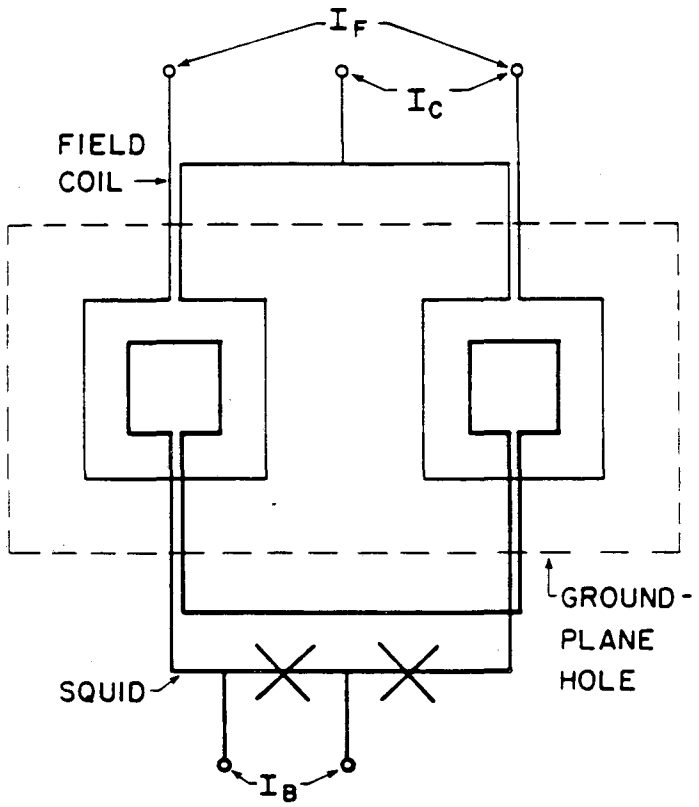

Fig.22 Thin-film miniature susceptometer (from ref. 74).

Awschalom and co-workers[33,75], have used a miniature susceptometer to perform magnetic spectroscopy of semiconductors with picosecond time-resolution. Linearly polarized pulses 4 ps in length are generated with a dye laser and split into a pump train and a weaker probe train. The time delay between the two trains can be varied, and each train is converted to circular polarization by a quarter-wave plate. The beams are chopped at 197 Hz and passed down an optical fiber to the sample in the cryostat. The pump pulses induce a magneto-optical susceptibility χ_{op} which is subsequently measured by means of the much weaker probe pulses of intensity δI that induce a magnetization $\chi_{op}\delta I$. The magnetization is detected by the SQUID at the chopping frequency, and its output is lock-in detected. By varying the time delay between the pump and probe pulses, one can investigate the dynamics of the induced magnetization. One also can vary the dye laser frequency through the red region of the visible spectrum to study the energy dependence of the magnetization. This technique recently has been extended to temperatures down to 0.3K[75].

C. Voltmeters

Probably the first practical application of a SQUID was to measure tiny, quasistatic voltages.[76] One simply connects the signal source -- for example a low resistance through which a current can be passed -- in series with a known resistance and the input coil of the SQUID. The output from the flux-locked loop is connected across the known resistance to obtain a null-balancing measurement of the voltage. The resolution is generally limited by Nyquist noise in the input circuit, which at 4.2 K varies from about 10^{-15} V $Hz^{-1/2}$ for a resistance of 10^{-8} Ω to about 10^{-10} V $Hz^{-1/2}$ for a resistance of 100 Ω.

Applications of these voltmeters range from the measurement of thermoelectric voltages and of quasiparticle charge imbalance in nonequilibrium superconductors to noise thermometry and the high precision comparison of the Josephson voltage-frequency relation in different superconductors.

D. The dc SQUID as a Radiofrequency Amplifier

Over recent years, the dc SQUID has been developed as a low noise amplifier for frequencies up to 100 MHz or more[77]. To understand the theory for the performance of this amplifier, we need to extend the theory of Sec.III by taking into account the noise associated with the current J(t) in the SQUID loop. For a bare SQUID with $\beta = 1$, $\Gamma = 0.05$ and $\Phi = (2n+1)\Phi_0/4$, one finds the spectral density of the current to be[78]

$$S_J(f) \approx 11\, k_B T/R. \tag{5.7}$$

Furthermore, the current noise is partially correlated with the voltage noise across the SQUID, the cross-spectral density being[78]

$$S_{VJ}(f) \approx 12\, k_B T. \tag{5.8}$$

The correlation arises, roughly speaking, because the current noise generates a flux noise which, in turn, contributes to the total voltage noise across the junction, provided $V_\Phi \neq 0$.

If one imagines coupling a coil to the SQUID, the coil will "see" an impedance Z in the SQUID loop that can be written in the form[79]

$$\frac{1}{Z} = \frac{1}{j\omega L} + \frac{1}{R}\,. \tag{5.9}$$

The dynamic inductance L and dynamic resistance R are not simply related to L and R, but vary with bias current and flux; for example, $1/L$ is zero for certain values of Φ.

One can make a tuned amplifier, for example, by connecting an input circuit to the SQUID, as shown in Fig.23. In general, the presence of this circuit modifies all of the SQUID parameters and the magnitude of the noise spectral densities.[80] Furthermore, the SQUID reflects an impedance $\omega^2 M_i^2/Z$ into the input circuit. Fortunately, however, one can neglect the mutual influence of the SQUID and input circuit, provided the coupling coefficient α^2 is sufficiently small, as it is under certain circumstances. For the purpose of illustration, we shall derive the noise temperature of the amplifier in Fig.23.

In the weak coupling limit, the noise current $J_N(t)$ induces a voltage $-M_i\dot{J}_N$ into the input circuit, and hence a current $-M_i\dot{J}_N / Z_i$, where

$$Z_i \approx R_i + j\omega L_i + 1/j\omega C_i \ . \tag{5.10}$$

Here, Z_i is the impedance of the input circuit and L_i and C_i are the series inductance and capacitance. The noise current in the input circuit, in turn, induces a flux $-M_i^2\dot{J}_N/Z_i$ in the SQUID loop and finally a voltage $-M_i^2\dot{J}_N V_\Phi/Z_i$ across the SQUID. Thus, the noise voltage across the SQUID in the presence of the input circuit is[77]

$$V_N'(t) = V_N(t) - M_i^2\dot{J}_N V_\Phi/Z_i \ , \tag{5.11}$$

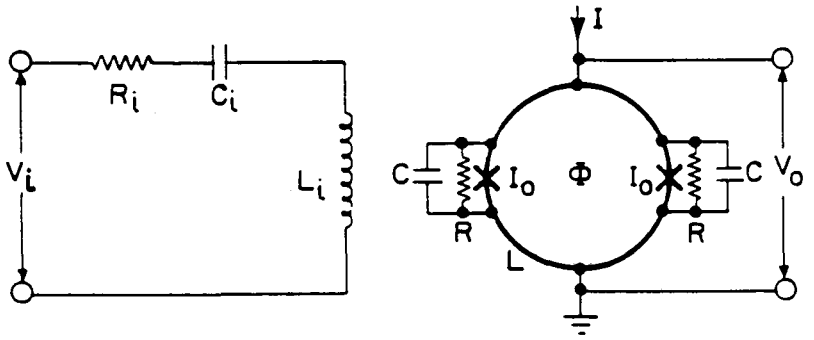

Fig.23 Tuned radiofrequency amplifier based on dc SQUID (from ref.77).

where $V_N(t)$ is the noise voltage of the bare SQUID, which we assume to be unchanged by the input circuit in the limit $\alpha^2 \to 0$. The spectral density of $V_N'(t)$ is easily found to be

$$S_v'(f) = S_v(f) + \frac{\omega^2 M_i^4 V_\Phi^2 S_J(f)}{|Z_i|^2} - \frac{2\omega M_i^2 V_\Phi(\omega L_i - 1/\omega C_i) S_{VJ}(f)}{|Z_i|^2} \cdot \quad (5.12)$$

We now suppose that we apply a sinusoidal input signal at frequency $\omega/2\pi$, with a mean-square amplitude $\langle V_i^2 \rangle$. The mean-square signal at the output of the SQUID is

$$\langle V_0^2 \rangle = M_i^2 V_\Phi^2 \langle V_i^2 \rangle / |Z_i|^2. \quad (5.13)$$

The signal-to-noise ratio is

$$S/N = \langle V_0^2 \rangle / S_v'(f) B \quad (5.14)$$

in a bandwidth B. It is convenient to introduce a noise temperature T_N for the amplifier by setting S/N = 1 with $\langle V_i^2 \rangle = 4k_B T_N R_i B$. This procedure implies that the output noise power generated by the SQUID is equal to the output noise power generated by the resistor R_i when it is at a temperature T_N. We then can optimize T_N with respect to R_i and C_i for a given value of L_i, and find

$$R_i^{(opt)} = \frac{\alpha^2 \omega L_i L V_\Phi}{S_V} (S_V S_J - S_{VJ}^2)^{1/2}, \quad (5.15)$$

$$\frac{1}{\omega C_i^{(opt)}} = \omega L_i \left(1 + \frac{\alpha^2 S_{VJ} L V_\Phi}{S_V}\right). \quad (5.16)$$

and

$$T_N^{(opt)} = \frac{\pi f}{k_B V_\Phi} (S_V S_J - S_{VJ}^2)^{1/2}. \quad (5.17)$$

We note from Eq.(5.16) that the optimum noise temperature occurs off-resonance. It often is more convenient in practice to use the amplifier at the resonant frequency of the tank circuit, given by $\omega^2 L_i C_i = 1$ (neglecting reflected components from the SQUID). In that case, one finds optimum values[77]

$$R_i^{(res)} = \alpha^2 \omega L_i L V_\Phi (S_J / S_V)^{1/2} \tag{5.18}$$

and

$$T_N^{(res)} = \frac{\pi f}{k_B V_\Phi} (S_V S_J)^{1/2}. \tag{5.19}$$

Using the results of Eqs.(3.7), (3.8), (5.7) and (5.8), we can write Eq.(5.18) in the form

$$\alpha^2 \omega L_i / R_i^{(res)} = \alpha^2 Q \approx 1. \tag{5.20}$$

This result shows that high-Q input circuits imply that α^2 is small, thereby justifying the assumption made at the beginning of this section. One also finds

$$T_N(f) \approx 18 f T / V_\Phi \approx 2 f \varepsilon(f) / k_B. \tag{5.21}$$

Thus, although $\varepsilon(f)$ does not fully characterize an amplifier, as noted earlier, within the framework of the model, it does enable one to predict T_N.

One can easily calculate the gain on resonance. For $\alpha^2 << 1$, an input signal V_i produces an output voltage $V_0 \approx (V_i / R_i^{(res)}) M_i V_\Phi$. The power gain is thus $G = (V_0^2/R_D)/(V_i^2/R_i)$, where R_d is the dynamic output resistance $(\partial V/\partial I)_\Phi$ of the SQUID. If we take $R_d \approx R$, we find

$$G \approx V_\Phi / \omega. \tag{5.22}$$

Hilbert and Clarke[77] made several radiofrequency amplifiers with both tuned and untuned inputs, flux biasing the SQUID near $\Phi = (2n + 1)\Phi_0/4$. There was no flux-locked loop. The measured parameters were in good agreement with predictions. For example, for an amplifier with $R \approx 8\ \Omega$, $L \approx 0.4$ nH, $L_i \approx 5.6$

nH, $M_i \approx 1$ nH and $V_\Phi \approx 3 \times 10^{10}$ sec^{-1} at 4.2 K, they found G = 18.6 ± 0.5 dB and T_N = 1.7 ± 0.5 K at 93 MHz. The predicted values were 17 dB and 1.1 K, respectively.

We emphasize that in this theory and these measurements one is concerned only with the noise temperature of the amplifier itself. Nyquist noise from the resistor adds a contribution which, in the example just given, exceeds the amplifier noise. Thus, the optimization procedure just outlined does not necessarily give the lowest system noise, and one would use a different procedure when the value of T_N in Eq.(5.17) or Eq.(5.19) is well below T.

In concluding this section, we comment briefly on the quantum limit for the dc SQUID amplifier. At T = 0, Nyquist noise in the shunt resistors should be replaced with zero point fluctuations [Eq.(2.11]. Koch et al.[81] performed a simulation in this limit and concluded that, within the limits of error, the noise temperature of a tuned amplifier in the quantum limit should be given by

$$T_N \approx hf/k_B \ln 2. \tag{5.23}$$

This is the result for any quantum-limited amplifier. The corresponding value for ε was approximately ħ, but it should be emphasized that quantum mechanics does not impose any precise lower limit on ε.[82] A number of SQUIDs have obtained noise energies of 3ħ or less, but there is no evidence as yet that a SQUID has attained quantum-limited performance as an amplifier.

E. Magnetic Resonance

SQUIDs have been used for two decades to detect magnetic resonance.[83] Most of the experiments involved the detection of magnetic resonance at low frequencies or the change in the static susceptibility of a sample induced by a resonance at high frequency. However, the development of the radiofrequency amplifier described in the previous section enables one to detect pulsed magnetic resonance directly at frequencies up to ~300 MHz.

Clarke, Hahn and co-workers have used the radiofrequency amplifier to perform nuclear quadrupole resonance[83] (NQR) and nuclear magnetic resonance[84] (NMR) experiments. They observed NQR in ^{35}Cl, which, in zero magnetic field, has two doubly-degenerate nuclear levels with a splitting of 30.6856 MHz. The experimental configuration is shown in Fig.24. The sample is placed in a superconducting pick-up coil, in series with which is an identical, counterwound coil. These coils are in series with an adjustable tuning capacitor

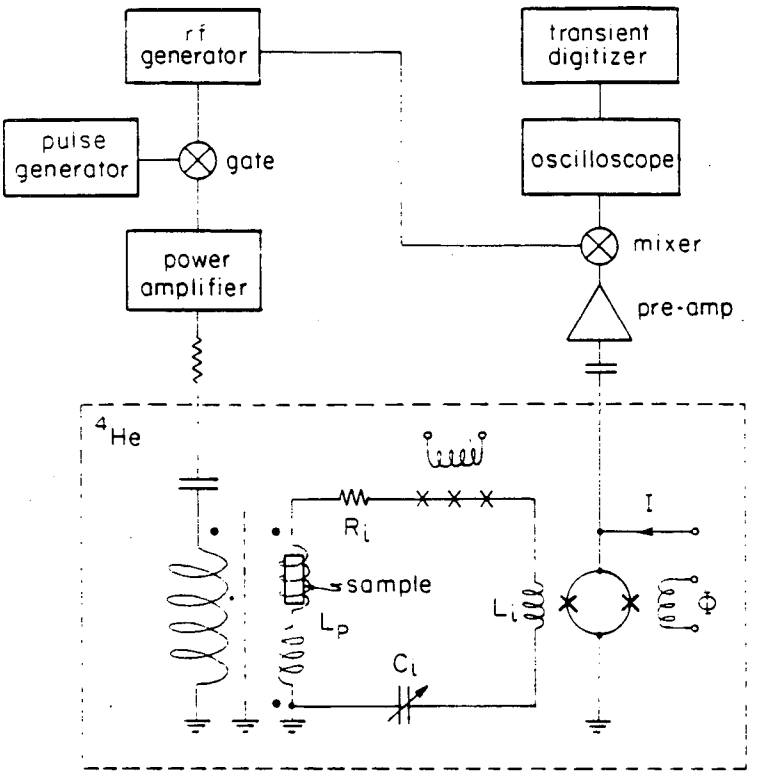

Fig.24 Circuit for NQR with dc SQUID amplifier (from ref. 83).

C_i, the 4-turn input coil of a planar dc SQUID and 20 unshunted Josephson junctions. The resistor R_i represents contact resistance and losses in the capacitor. Radiofrequency pulses applied to the transmitter coil cause the nuclear spins to precess; after each pulse is turned off, the amplifier detects the precessing magnetization. The amplified signal is mixed down with a reference provided by the rf generator, and the mixed-down signal is passed through a low-pass filter, observed on an oscilloscope, and recorded digitally for further analysis.

The major difficulty with this technique, and indeed with other pulsed methods, is the saturation of the amplifier by the very large rf pulse. In the present experiments, the effects of this pulse are reduced in two ways. First, the gradiometer-like configuration gives a common-mode rejection that can be as high as 3×10^4. Second, the series of junctions in the input circuit acts as a Q-spoiler[83]. As the current begins to build in the tuned circuit, the junctions switch to the resistive state with a total resistance of about 1 kΩ, thereby reducing the Q to ~ 1. When the pulse is turned off, the transients die out very quickly and the junctions revert to their zero voltage state, rapidly restoring Q to its full value,

usually several thousand. In this way, one can combine the benefits of a high-Q tuned circuit and a sensitive amplifier while retaining a relatively short dead-time after each pulse. In their initial experiments, Hilbert et al.[83] achieved a resolution for a single pulse of ~2 x 10^{16} spins (~2 x 10^{16} nuclear Bohr magnetons) in a bandwidth of 10 kHz.

Subsequently, the Q-spoiler and SQUID amplifier were used to detect atomic polarization induced by precessing nuclear electric quadrupoles.[85] In this experiment, the $NaClO_3$ sample was placed in a capacitor that formed part of the tuned input circuit, and NQR induced in the usual way by radiofrequency pulses. The precessing electric quadruple moments induce a net electric dipole moment in the neighboring atoms, provided the crystal is non-centrosymmetric. These dipole moments, in turn, produce an oscillating electric polarization in the crystal and hence a voltage on the capacitor that is amplified in the usual way. This technique yields information on the location and polarization of atoms near nuclear quadruple moments.

The Q-spoiler and amplifier also have been used to detect nuclear magnetic resonance[84]. In these experiments one applies a magnetic field with an amplitude of several tesla to the crystal, and places the superconducting circuitry some distance away in a relatively low field. In yet another experiment, Sleator et al.[86] observed "spin noise" in ^{35}Cl. An rf signal at the NQR frequency equalized the populations of the two nuclear spin levels, and then was turned off to leave a zero-spin state. A SQUID amplifier (without a Q-spoiler) was able to detect the photons emitted spontaneously as the upper state decayed, even though the lifetime per nucleus for this process was ~ 10^6 centuries. The detected power was about 5 x 10^{-21}W in a bandwidth of about 1.3 kHz.

F. Gravity Wave Antennas

A quite different application of SQUIDs is the detection of minute displacements, such as those of the bar in a gravity wave antenna.[87,88] About a dozen groups worldwide are using these antennas to search for the pulse of gravitational radiation that is expected to be emitted when a star collapses. The radiation induces longitudinal oscillations in the large, freely suspended bar, but because the amplitude is very tiny, one requires the sensitivity of a dc SQUID to detect it. As an example, we briefly describe the antenna at Stanford University, which consists of an aluminum bar 3 meters long (and weighing 4800 kg) suspended in a vacuum chamber at 4.2 K. The fundamental longitudinal mode is at $\omega_a/2\pi \approx 842$ Hz, and the Q is 5 x 10^6. The transducer is shown schematically in

Fig.25. A circular niobium diaphragm is clamped at its perimeter to one end of the bar, with a flat spiral coil made of niobium wire mounted on each side. The two coils are connected in parallel with each other and with the input coil of a SQUID; this entire circuit is superconducting. A persistent supercurrent circulates in the closed loop formed by the two spiral coils. The associated magnetic fields exert a restoring force on the diaphragm so that by adjusting the current, one can set the resonant frequency of the diaphragm equal to that of the bar. A longitudinal oscillation of the bar induces an oscillation in the position of the diaphragm relative to the two coils, thereby modulating their inductances. As a result of flux quantization, a fraction of the stored supercurrent is diverted into the input coil of the SQUID, which detects it in the usual way.

The present Stanford antenna has a root-mean-square strain sensitivity $<(\delta\ell)^2>^{1/2}/\ell$ of 10^{-18}, where ℓ is the length of the bar, and $\delta\ell$ is its longitudinal displacement. This very impressive sensitivity, which is limited by thermal noise in the bar, is nonetheless adequate to detect events only in our own galaxy. Because such events are rare, there is very strong motivation to make major improvements in the sensitivity.

If the bar could be cooled sufficiently, the strain resolution would be limited only by the bar's zero-point motion and would have a value of about 3×10^{-21}. At first sight one might expect that the bar would have to be cooled to

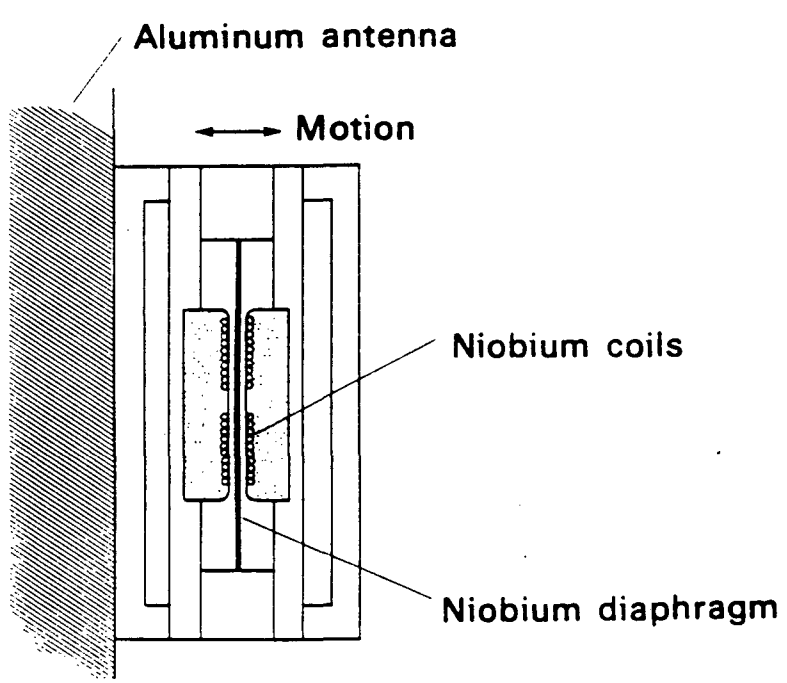

Fig.25 Transducer for gravity wave antenna (courtesy P.F. Michelson).

an absurdly low temperature to achieve this quantum limit, because a frequency of 842 Hz corresponds to a temperature $\hbar\omega_a/k_B$ of about 40 nK. However, it turns out that one can make the effective noise temperature T_{eff} of the antenna much lower than the temperature T of the bar. If a gravitational signal in the form of a pulse of length τ_S interacts with an antenna that has a decay time Q/ω_a, then the effective noise temperature is given approximately by the product of the bar temperature and the pulse length divided by the decay time: $T_{eff} \approx \tau_S\omega_a T/Q$. Thus, one can make the effective noise temperature much less than the temperature of the bar by increasing the bar's resonant quality factor sufficiently. To achieve the quantum limit, in which the bar energy $\hbar\omega_a$ is greater than the effective thermal energy $k_B T_{eff}$, one would have to lower the temperature T below $Q\hbar/k_B\tau_S$, which is about 40 mK for a quality factor Q of 5×10^6 and a pulse length τ_S of 1 msec. One can cool the antenna to this temperature with the aid of a large dilution refrigerator.

Needless to say, to detect the motion of a quantum-limited antenna, one needs a quantum-limited transducer, a requirement that has been the major driving force in the development of ultra-low-noise dc SQUIDs. As we have seen, however, existing dc SQUIDs at low temperatures are now within striking distance of the quantum limit, and there is every reason to believe that one will be able to operate an antenna quite close to the quantum limit within a few years.

G. Gravity Gradiometers

The gravity gradiometer, which also makes use of a transducer to detect minute displacements, has been pioneered by Paik[89] and Mapoles[90]. The gradiometer consists of two niobium proof masses, each constrained by springs to move along a common axis (Fig.26). A single-layer spiral coil of niobium wire is attached to the surface of one of the masses so that the surface of the wire is very close to the opposing surface of the other mass. Thus, the inductance of the coil depends on the separation of the two proof masses, which, in turn, depends on the gravity gradient. The coil is connected to a second superconducting coil which is coupled to a SQUID via a superconducting transformer. A persistent supercurrent, I, maintains a constant flux in the detector circuit. Thus, a change in the inductance of the pick-up coil produces a change in I, and hence, a flux in the SQUID that is related to the gravity gradient. More sophisticated versions of this design enable one to balance the restoring forces of the two springs electronically,[90] thereby eliminating the response to an

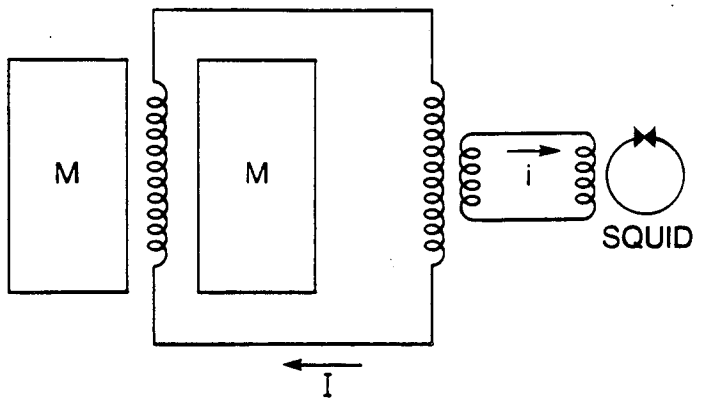

Fig.26 Gravity gradiometer showing two proof masses (M) on either side of a planar spiral coil (from ref. 90).

acceleration (as opposed to an acceleration gradient). Sensitivities of a few Eötvös $Hz^{-1/2}$ have been achieved at frequencies above 2 Hz.

Instruments of this kind could be used to map the earth's gravity gradient, and may be used to test the inverse gravitational square law and in inertial navigation.

VI. THE IMPACT OF HIGH TEMPERATURE SUPERCONDUCTIVITY

The advent of the high-transition-temperature (T_C) superconductors[91] has stimulated great interest in the prospects for superconducting devices operating at liquid (LN) temperature (77 K). Indeed, a number of groups have already successfully operated such SQUIDs. In this section I shall give a brief overview of this work.

A. Predictions for White Noise

In designing a SQUID for operation at LN temperature, one must bear in mind the constraints imposed by thermal noise on the critical current and inductance, $I_0 \gtrsim 10\pi k_B T/\Phi_0$ and $L \lesssim \Phi_0^2/5k_B T$. For T =77 K, we find $I_0 \gtrsim 16\ \mu A$ and $L \lesssim 0.8$ nH. If we take as arbitrary but reasonable values, L = 0.2 nH and $I_0 = 20\ \mu A$, we obtain $2LI_0/\Phi_0 = 4$ for the dc SQUID and $LI_0/\Phi_0 = 2$ for the rf SQUID. These values are not too far removed from optimum, and

to a first approximation, we can use the equations for the noise energy given in Secs. III and IV.

For the case of the dc SQUID, the noise energy is predicted by either Eq.(3.9) or Eq.(3.10). However, since nobody has yet made a Josephson tunnel junction with high-T_C materials, it is somewhat unrealistic to use Eq.(3.10), which involves the junction capacitance, and instead we use Eq.(3.9). The value of R is an open question, and we rather arbitrarily adopt 5 Ω, which is not too different from values achieved experimentally for high-T_C grain boundary junctions.[92] With L = 0.2 nH, T = 77 K and R = 5 Ω, Eq.(3.9) predicts $\varepsilon \approx 4 \times 10^{-31}$ J Hz^{-1}. This value is only about one order of magnitude higher that that found at 4.2 K for typical Nb-based, thin-film dc SQUIDs, and is somewhat better than that found in commercially available toroidal SQUIDs. These various values are summarized in Fig.27. If one could actually achieve the predicted resolution in a SQUID at 77 K at frequencies down to 1 Hz or less, it would be adequate for most of the applications discussed in Sec. V.

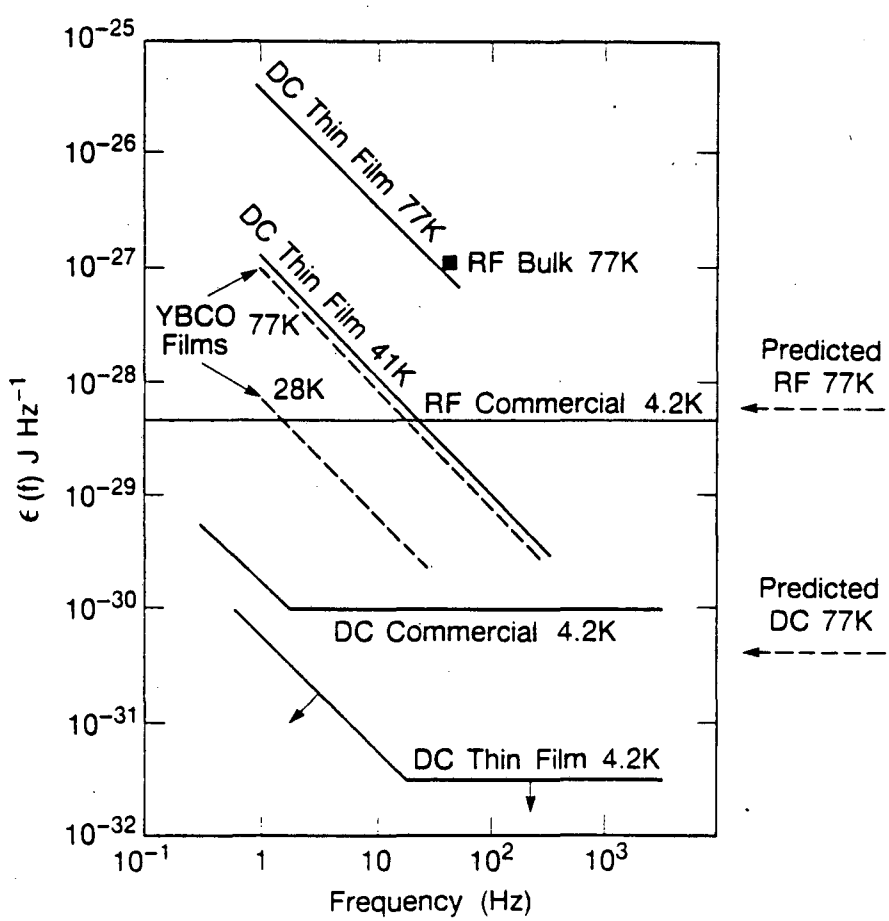

Fig.27 Noise energy ε(f) vs. frequency for several SQUIDs and for a YBCO film.

For the rf SQUID, Eq.(4.10) predicts an intrinsic noise energy of about 6×10^{-29} J Hz^{-1} for $I_0 = 20\ \mu A$, $LI_0 = 2\Phi_0$, $\omega_{rf}/2\pi = 20$ MHz and T = 77 K. This value is comparable with the overall value obtained experimentally with 4.2 K devices where the effective noise temperature T_a^{eff} of the preamplifier and tank circuit is much higher than the bath temperature for the case in which the preamplifier is at room temperature - see Sec.IV. B. However, when one operates a SQUID at 77 K, there is no reason for T_a^{eff} to increase and the system noise energy should be comparable with that at 4.2K.

With regard to 1/f noise, in general, one might expect both critical current noise and flux noise to contribute. However, it seems impractical to make any a priori predictions of the magnitude of these contributions.

B. Practical Devices

Although a number of dc and rf SQUIDs have been made from YBCO, I shall describe just one of each type. It appears that the first dc SQUID was made by Koch et al.[92] In their devices, they patterned the films by covering the regions of YBCO destined to remain superconducting with a gold film, and ion implanted the unprotected regions so that they became insulators at low temperatures. The configuration is shown in Fig.28. The estimated inductance is 80 pH. The two microbridges exhibited Josephson-like behavior, which actually arose from junctions formed by grain boundaries between randomly oriented grains of YBCO. As the quality of the films has improved, conventional patterning techniques such as lift off and ion etching have become possible. The I-V characteristics of these devices are modulated by an applied flux, although the

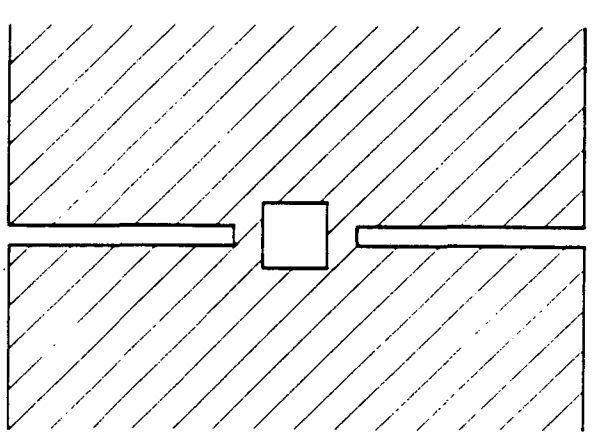

Fig.28 Planar thin-film dc SQUID fabricated from YBCO (re-drawn from ref. 92).

C. Flux Noise in YBCO Films

It is evident that the 1/f noise level in YBCO SQUIDs is very high compared with that in Nb or Pb devices at 4.2K. Ferrari et al.[94] have investigated the source of this noise by measuring the flux noise in YBCO films. Each film, deposited on a $SrTiO_3$ chip, was patterned into a loop and mounted parallel and very close to a Nb-based SQUID (with no input coil) so that any flux noise in the YBCO loop could be detected by the SQUID. The assembly was enclosed in a vacuum can immersed in liquid helium. The SQUID was maintained at 4.2 K, while the temperature of the YBCO film could be increased by means of a resistive heater. Below T_C, the spectral density of the flux noise scaled as 1/f over the frequency range 1 to 10^3 Hz, and increased markedly with temperature. Three films were studied, with microstructure improving progressively with respect to the fraction of grains oriented with the c-axis perpendicular to the substrate. The critical current density correspondingly increased, to a value of 2×10^6 Acm^{-2} at 4.2 K in the best film. The spectral density of the noise measured at 1Hz is shown vs. temperature in Fig.30. We see that in each case the noise increases rapidly as the temperature approaches T_C, and that, at a given

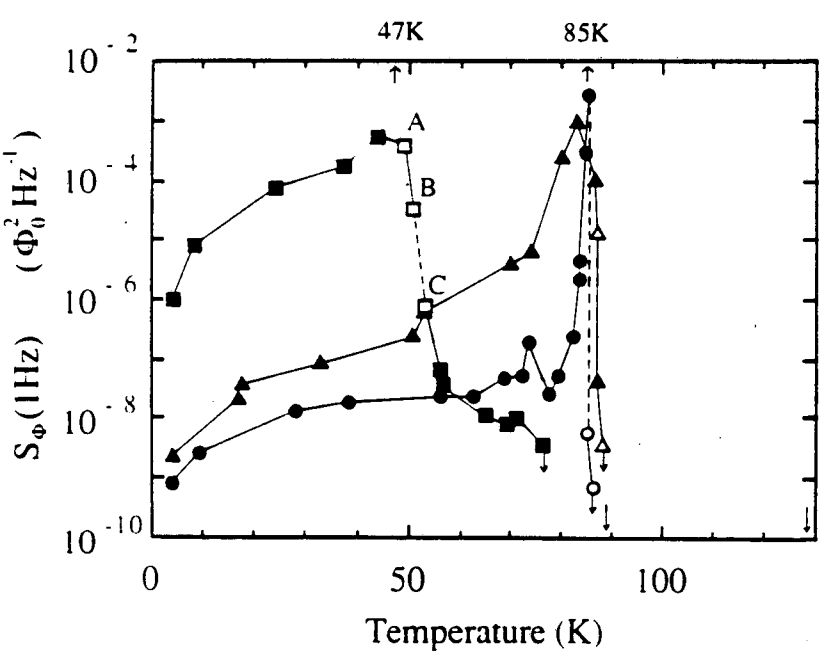

Fig.30 Spectral density of flux noise at 1Hz vs. temperature for three YBCO films: polycrystalline (squares), mixed a- and c-axis (triangles) and >90% c-axis (circles). Solid symbols indicate the noise is 1/f at 1Hz, open that it is white or nearly white (from ref. 94).

V-Φ curves are often hysteretic and nonperiodic, probably because of flux trapped in the YBCO films. The noise energy scaled approximately as 1/f over the frequency range investigated, usually 1 to 10^3 Hz. The lowest noise energies achieved to date at 1 Hz are 4×10^{-27} J Hz^{-1} at 41 K and, in a different device, 2×10^{-26}J/Hz at 77 K. These values are plotted in Fig.27.

The best characterized rf SQUID reported so far is that of Zimmerman et al.[93] They drilled a hole along the axis of a cylindrical pellet of YBCO, and cut a slot part way along a radius (Fig.29). The pellet was glued into an aluminum holder, also with a slot, and the assembly was immersed in LN. A taper pin forced into the slot in the mount caused the YBCO to break in the region of the cut; when the pin was withdrawn slightly, the YBCO surfaces on the two sides of the crack were brought together, forming a "break junction". The rf SQUID so formed was coupled to a resonant circuit and operated in the usual way. The best flux resolution was $4.5 \times 10^{-4}\ \Phi_0\ Hz^{-1/2}$ at 50 Hz, corresponding to a noise energy of 1.6×10^{-27} J Hz^{-1} for L = 0.25 nH - see Fig.27.

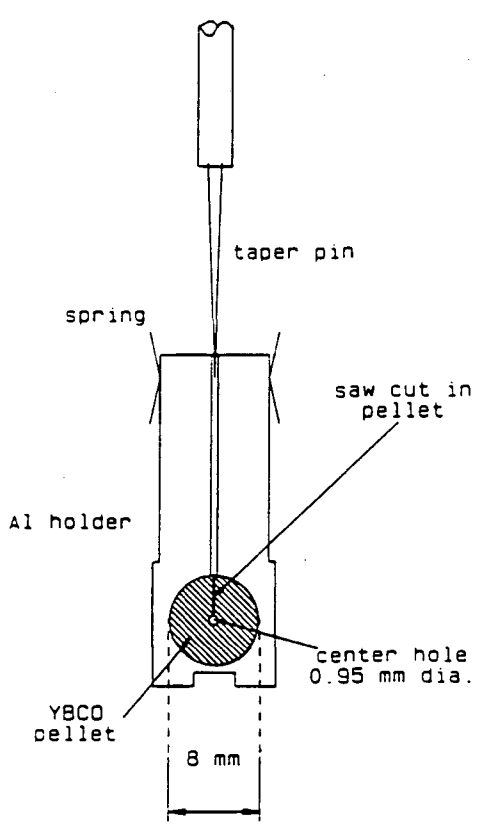

Fig. 29 Break-junction rf SQUID (from ref. 93).

temperature, the noise decreases dramatically as the quality of the films is improved. The noise energy estimated at 28 K and 77 K with an assumed inductance of 400 pH is shown in Fig.27.

These results demonstrate that YBCO films are intrinsically noisy. The noise presumably arises from the motion of flux quanta trapped in the films, possibly at grain boundaries. This mechanism is almost certainly the origin of the l/f noise observed in YBCO SQUIDs, and, in general terms, is similar to the origin of l/f flux noise in Nb SQUIDs. It is encouraging that the noise is reduced as the microstructure of the films is improved, and it should be emphasized that there is no reason to believe the lowest noise measured so far represents a lower bound. The implications are that SQUIDs and flux transformers coupled to them should be made of very high quality films.

D. Future Prospects for High-T_c SQUIDs

One rather obvious application of a high-T_C SQUID is as a geophysical magnetometer - see Sec.V.A. At the moment, however, it is not entirely straightforward to predict the performance, since the devices are still evolving, and it is evident from the noise measurements on YBCO films that thin-film flux transformers may introduce considerable levels of low frequency noise. To make an estimate, we assume that we can optimally couple the 77 K dc SQUID with the noise energy shown in Fig.27 to a <u>noiseless</u> flux transformer with a thin-film pick-up loop with a diameter of 50 mm. The estimated loop inductance is about 150 nH. Using Eq.(5.6), we find a magnetic field resolution of roughly 0.1 pT $Hz^{-1/2}$ at 1 Hz, improving to 0.01 pT $Hz^{-1/2}$ at 100 Hz. Although this performance is quite good, one should realize that commercially available coils operated at room temperature offer a resolution of about 0.03 pT $Hz^{-1/2}$ over this frequency range. Furthermore, our assumption of a noise-free flux transformer is rather optimistic. Nonetheless, given the short time over which the high-T_C materials have been available, one should be rather encouraged: a relatively modest reduction in the l/f noise that might be gained from improving the quality of YBCO films or even from using alternate materials might yield a useful geophysical device.

One might note here that the real advantage in using liquid nitrogen as opposed to liquid helium for field applications, is not really the reduction in cost, a savings which is negligible compared with the cost of mounting a field operation, but rather is the very much slower boil-off rate of liquid nitrogen. The latent heat of vaporization of liquid N_2 is about 60 times that of liquid ^4He, so

that one should be able to design cryostats of modest size with hold-times of up to a year. It also is noteworthy that liquid Ne, which boils at 27 K, has a latent heat roughly 40 times that of liquid He, and its use also would greatly extend the running time over that of liquid He, for roughly the same cost per day. We see from Fig.30 that the 1/f noise in YBCO films can be considerably lower at 27 K than at 77 K, so that the lower temperature operation could be a considerable advantage.

The likely impact of high-T_C SQUIDs on the more demanding neuromagnetic applications is much smaller, at least for the near future. Here, one needs very high sensitivity at frequencies down to 0.1 Hz or less, but is not particularly concerned with the cost of liquid ^{4}He or the need to replenish it every day or two. Furthermore, low-noise, closed-cycle refrigerators are just becoming available that obviate the need to supply liquid cryogens in environments where electrical power is readily available. Thus, it is difficult to imagine that high-T_C SQUIDs will have a significant impact in this area unless there is a major reduction in the 1/f noise.

In concluding this section, we note that two key problems must be solved before high-T_C SQUIDs are likely to become technologically important. The first is the development of a reproducible and reliable Josephson junction. Although great progress has been made with grain boundary junctions, it is not clear that one can base a technology on this technique. Shiota et al.[95] have reported YBCO-insulator-YBCO junctions formed by fluorination of the base electrode, but the I-V characteristics revealed that one of the surfaces was normal. It is hoped that it will be possible to produce all-YBCO junctions exhibiting Josephson tunneling in the near future. An alternative might be a superconductor-normal metal-superconductor junction.[96] The second problem is concerned with the reduction of hysteresis and noise in thin films of high-T_C material. The motion of magnetic flux in the films is responsible for both effects, and one has to learn to produce films with lower densities of flux lines or higher pinning energies. Given the world-wide effort on the new superconductors, there is every reason to be optimistic about the long-term future of SQUIDs based on these materials.

VII. CONCLUDING REMARKS

In this chapter I have tried to give an overview of the current status of dc and rf SQUIDs. I make no pretence that this account is comprehensive. There are many SQUID designs and applications that I have not mentioned, but I hope that I have given some flavor of the amazing versatility of these devices. I find it remarkable that SQUIDs are the basis of both the most sensitive magnetometer available at 10^{-4} Hz and the lowest noise radio frequency amplifier at 10^{8} Hz.

It is somewhat ironic that the best developed devices, thin-film dc SQUIDs, are still not commercially available. This seemingly lamentable state of affairs simply reflects supply and demand. If thin-film SQUIDs were cheaper, people would buy them, and if people would buy them thin-film SQUIDs would be cheaper. The basic problem is that the demand for these devices has not yet been sufficient to convince a company to produce them on a large enough scale to bring the price down to an affordable level. However, some 14 years after low noise dc SQUIDs were first demonstrated, I believe that the situation is finally about to change. After all, one needs only a single major application to make reasonably-priced SQUIDs available for any number of applications, and there now seem to be two such major applications on the horizon. The first is in neuromagnetism: if this application is to become a clinical reality, one will need systems with as many as 100 channels, and the need for 100 channels will inevitably lead to the production of thin-film SQUIDs on a large scale. The second is the advent of high-T_C thin-film SQUIDs. If these devices attain sufficient sensitivity and reliability for geophysical applications, not to mention laboratory-based applications such as voltmeters, they will be in sufficient demand to justify production on a commercial basis.

Either way, I think the next few years are going to be particularly interesting.

ACKNOWLEDGMENTS

I am indebted to D. Crum for supplying Fig. 21(a), P.F. Michelson Fig. 25, D. Paulsen Fig. 19, F. C. Wellstood Fig. 10, and J. E. Zimmerman Fig. 29. For that part of the work carried out at Berkeley, I wish to thank the following for their hard work and dedication: Gordon Donaldson, Wolf Goubau, Mike Heaney, Claude Hilbert, Cristof Heiden, Mark Ketchen, Roger Koch, John Martinis, Bonaventura Savo, Claudia Tesche, Cristian Urbina,

Dale Van Harlingen and Fred Wellstood. I thank in particular Roger Koch and Fred Wellstood for helpful conversations during the preparation of this manuscript.

This work was supported by the Director, Office of Energy Research, Office of Basic Energy Sciences, Materials Sciences Division of the U.S. Department of Energy under contract number DE-AC03-76SF00098.

REFERENCES

1. London. F.: Superfluids. Wiley, New York 1950
2. Josephson. B.D.: Possible new effects in superconductive tunneling. Phys. Lett. **1**. 251-253 (1962); Supercurrents through barriers. Adv. Phys. **14**. 419-451 (1965)
3. Jaklevic. R.C., Lambe. J., Silver. A.H., and Mercereau. J.E.: Quantum interference effects in Josephson tunneling. Phys. Rev Lett. **12**. 159-160 (1964)
4. Zimmerman. J.E., Thiene. P., Harding. J.T.: Design and operation of stable rf-biased superconducting point-contact quantum devices, and a note on the properties of perfectly clean metal contacts. J. Appl. Phys. **41**. 1572-1580 (1970)
5. Mercereau, J.E.: Superconducting magnetometers. Rev. Phys. Appl. **5**. 13-20 (1970); Nisenoff. M.: Superconducting magnetometers with sensitivities approaching 10^{-10} gauss. Rev. Phys. Appl. **5**. 21-24 (1970)
6. Stewart. W.C.: Current-voltage characteristics of Josephson junctions. Appl. Phys. Lett. **12**. 277-280 (1968)
7. McCumber. D.E.: Effect of ac impedance on dc voltage-current characteristics of Josephson junctions. J. Appl. Phys. **39**. 3113-3118 (1968).
8. Ambegaokar. V. and Halperin. B. I.: Voltage due to thermal noise in the dc Josephson effect. Phys. Rev. Lett. **22**. 1364-1366 (1969)
9. Clarke. J. and Koch. R. H.: The impact of high-temperature superconductivity on SQUIDs. Science **242**. 217-223 (1988)
10. Likharev. K. K. and Semenov. V. K.: Fluctuation spectrum in superconducting point junctions. Pis'ma Zh. Eksp. Teor. Fiz. **15**. 625-629 (1972). [JETP Lett. **15**. 442-445 (1972)]
11. Vystavkin. A. N., Gubankov. V.N., Kuzmin. L.S., Likharev. K.K., Migulin. V.V. and Semenov. V.K.: S-c-s junctions as nonlinear elements of microwave receiving devices. Phys. Rev. Appl. **9**. 79-109 (1974)
12. Koch. R.H., Van Harlingen. D.J. and Clarke. J.: Quantum noise theory for the resistively shunted Josephson junction. Phys. Rev Lett. **45**. 2132-2135 (1980)
13. Tesche. C.D. and Clarke. J.: dc SQUID: Noise and Optimization. J. Low. Temp. Phys. **27**. 301-331 (1977)

14. Bruines. J.J.P., de Waal. V.J. and Mooij. J.E.: Comment on "dc SQUID noise and optimization" by Tesche and Clarke. J. Low. Temp. Phys. **46**. 383-386 (1982)
15. De Waal. V.J., Schrijner. P. and Llurba. R. Simulation and optimization of a dc SQUID with finite capacitance. J. Low. Temp. Phys. **54**. 215-232 (1984)
16. Ketchen. M.B. and Jaycox. J.M.: Ultra-low noise tunnel junction dc SQUID with a tightly coupled planar input coil. Appl. Phys. Lett. **40**. 736-738 (1982)
17. Jaycox J.M. and Ketchen M.B.: Planar coupling scheme for ultra low noise dc SQUIDs. IEEE Trans. Magn., **MAG- 17**. 400-403 (1981)
18. Wellstood. F.C., Heiden. C. and Clarke. J.: Integrated dc SQUID magnetometer with high slew rate. Rev. Sci. Inst. **55**. 952-957 (1984)
19. Gurvitch. M., Washington. M.A. and Huggins. H.A.: High quality refactory Josephson tunnel junction utilizing thin aluminum layers. Appl. Phys. Lett. **42**. 472-474 (1983)
20. De Waal. V.J., Klapwijk. T.M. and Van den Hamer. P.: High performance dc SQUIDs with submicrometer niobium Josephson junctions. J. Low. Temp. Phys. **53**. 287-312 (1983)
21. Tesche. C.D., Brown. K.H., Callegari. A.C., Chen. M.M., Greiner. J.H., Jones. H.C., Ketchen. M.B., Kim. K.K., Kleinsasser. A.W., Notarys. H.A., Proto. G., Wang. R.H. and Yogi. T.: Practical dc SQUIDs with extremely low l/f noise. IEEE Trans. Magn. **MAG-21.** 1032-1035 (1985)
22. Pegrum. C.M., Hutson. D., Donaldson. G.B. and Tugwell. A.: DC SQUIDs with planar input coils. ibid. 1036-1039 (1985)
23. Noguchi. T., Ohkawa. N. and Hamanaka. K.: Tunnel junction dc SQUID with a planar input coil. SQUID 85 Superconducting Quantum Interference Devices and their Applications. Ed. Hahlbohm. H. D. and Lubbig. H. (Walter de Gruyter, Berlin, 1985) 761-766
24. Muhlfelder. B., Beall. J.A., Cromar. M.W. and Ono. R.H.: Very low noise tightly coupled dc SQUID amplifiers. Appl. Phys. Lett. **49**. 1118-1120 (1986)
25. Knuutila. J., Kajola. N., Seppä. H., Mutikainen. R. and Salmi. J.: Design, optimization and construction of a dc SQUID with complete flux transformer circuits. J. Low. Temp. Phys. **71**. 369-392 (1988)
26. Carelli. P. and Foglietti. V.: Behavior of a multiloop dc superconducting quantum interference device. J. Appl. Phys. **53**. 7592-7598 (1982)
27. Clarke. J., Goubau. W.M. and Ketchen. M.B.: J. Low. Temp. Phys. **25**. 99-144 (1976)
28. Ketchen. M.B., Goubau. W.M., Clarke. J. and Donaldson. G.B.: Superconducting thin-film gradiometer. J. Appl. Phys. **44**. 4111-4116 (1978)
29. Wellstood. F.C., and Clarke. J.: unpublished.

30. Wellstood. F.C., Urbina. C. and Clarke. J.: Low-frequency noise in dc superconducting quantum interference devices below 1K. Appl. Phys. Lett. **50**. 772-774 (1987)
31. Roukes. M. L., Freeman. M. R., Germain. R. S., Richardson. R. C. and Ketchen. M. B.: Hot electrons and energy transport in metals at millikelvin temperatures. Phys. Rev. Lett. **55.** 422-425 (1985)
32. Wellstood. F.C., Urbina. C. and Clarke. J.: Hot electron effect in the dc SQUID. Proceedings of the Applied Superconductivity Conference August 21-25 1988 (to be published).
33. Ketchen. M.B., Awschalom. D.D., Gallagher. W.J., Kleinsasser. A.W., Sandstrom. R.L., Rozen. J.R. and Bumble. B.: Design, fabrication and performance of integrated miniature SQUID susceptometers. Proceedings of the Superconductivity Conference August 21-25 1988 (to be published).
34. Koch. R.H., Clarke. J., Goubau. W.M., Martinis. J.M., Pegrum. C.M. and Van Harlingen. D.J.: Flicker (l/f) noise in tunnel junction dc SQUIDs. J. Low. Temp. Phys. **51**. 207-224 (1983)
35. Rogers. C.T. and Buhrman. R.A.: Composition of l/f noise in metal-insulator-metal tunnel junctions. Phys. Rev. Lett. **53**. 1272-1275 (1984)
36. Dutta. P. and Horn. P.M.: Low-frequency fluctuations in solids: l/f noise. Rev. Mod. Phys. **53**. 497-516 (1981)
37. Savo. B., Wellstood. F.C. and Clarke. J.: Low-frequency excess noise in Nb-Al_2O_3-Nb Josephson tunnel junction. Appl. Phys. Lett. **50**. 1757-1759 (1987)
38. Tesche. C.D., Brown. R. H., Callegari. A. C., Chen. M. M., Greiner. J. H., Jones. H. C., Ketchen. M. B., Kim. K. K., Kleinsasser. A. W., Notarys. H. A., Proto. G., Wang. R. H. and Yogi. T.: Well-coupled dc SQUID with extremely low l/f noise. Proc. 17th International Conference on low temperature physics LT-17. (North Holland, Amsterdam 1984) 263-264
39. Foglietti. V, Gallagher. W. J., Ketchen. M. B., Kleinsasser. A. W., Koch. R. H., Raider. S. I. and Sandstrom. R. L.: Low-frequency noise in low l/f noise dc SQUIDs. Appl. Phys. Lett. **49**. 1393-1395 (1986).
40. Biomagnetic Technologies Inc. 4174 Sorrento Valley Blvd., San Diego, CA 92121.
41. Fujimaki. N., Tamura. H., Imamura. T. and Hasuo. S.: A single-chip SQUID magnetometer. Digest of Tech. papers of 1988 International Solid-state conference. (ISSCC) San Francisco. pp. 40-41. A longer version with the same title is to be published.
42. Drung. D.: Digital Feedback loops for dc SQUIDs. Cryogenics **26.** 623-627 (1986). Drung. D., Crocoll. E., Herwig. R., Neuhaus. M. and Jutzi. W.: Measured performance parameters of gradiometers with digital output. Proceedings of the Applied Superconductivity Conference, August 21-25 1988 (to be published).

43. Mück. M. and Heiden. C.: Simple dc SQUID system based on a frequency modulated relaxation oscillator. Proceedings of the Applied Superconductivity Conference, August 21-25 1988 (to be published).
44. Clarke. J.: Superconducting QUantum Interference Devices for Low Frequency Measurements. Superconductor Applications : SQUIDs and Machines, Ed. Schwartz. B. B.and Foner. S. (Plenum New York 1977). pp 67-124.
45. Giffard. R. P., Webb. R.A. and Wheatley. J.C.: Principles and methods of low-frequency electric and magnetic measurements using rf-biased point-contact superconducting device. J. Low. Temp. Phys. **6**. 533-610 (1972)
46. Kurkijärvi. J.: Intrinsic fluctuations in a superconducting ring closed with a Josephson junction. Phys. Rev. B **6**. 832-835 (1972)
47. Kurkijärvi. J. and Webb. W.W.: Thermal noise in a superconducting flux detector. Proc. Applied Superconductivity Conf. (Annapolis, MD.) 581-587 (1972)
48. Jackel. L.D. and Buhrman. R.A.: Noise in the rf SQUID. J. Low. Temp. Phys. **19**. 201-246 (1975)
49. Ehnholm. G.J.: Complete linear equivalent circuit for the SQUID. SQUID Superconducting Quantum Interference Devices and their Applications. Ed. Hahlbohm. H.D. and Lubbig. H. (Walter de Gruyter, Berlin, 1977) 485-499; Theory of the signal transfer and noise properties of the rf SQUID. J. Low. Temp. Phys. **29**. 1-27(1977)
50. Hollenhorst. H.N. and Giffard. R.P.: Input noise in the hysteretic rf SQUID: theory and experiment. J. Appl. Phys. **51**. 1719-1725 (1980)
51. Kurkijärvi. J.: Noise in the superconducting flux detector. J. Appl. Phys. **44**. 3729-3733 (1973)
52. Giffard. R.P., Gallop. J.C. and Petley. B.N.: Applications of the Josephson effects. Prog. Quant. Electron **4**. 301-402 (1976)
53. Ehnholm. G.J., Islander. S.T., Ostman. P. and Rantala. B.: Measurements of SQUID equivalent circuit parameters. J. de Physique **39**. colloque C6. 1206-1207 (1978)
54. Giffard. R.P. and Hollenhorst. J.N.: Measurement of forward and reverse signal transfer coefficients for an rf-biased SQUID. Appl. Phys. Lett. **32**. 767-769 (1978)
55. Jackel. L. D., Webb. W. W., Lukens. J. E. and Pei. S. S.: Measurement of the probability distribution of thermally excited fluxoid quantum transitions in a superconducting ring closed by a Josephson junction. Phys. Rev. **B9**. 115-118 (1974)
56. Long. A., Clark. T. D., Prance. R. J. and Richards. M. G.: High performance UHF SQUID magnetometer. Rev. Sci. Instrum. **50**. 1376-1381 (1979)
57. Hollenhorst. J. N. and Giffard. R. P.: High sensitivity microwave SQUID. IEEE Trans. Magn. **MAG-15**. 474-477 (1979)

58. Ahola. H., Ehnholm. G. H., Rantala. B. and Ostman. P.: Cryogenic GaAs-FET amplifiers for SQUIDs. J. de Physique **39**. colloque C6. 1184-1185 (1978); J. Low Temp. Phys. **35**. 313–328 (1979)
59. For a review, see Clarke. J.: Advances in SQUID Magnetometers. IEEE Trans. Election Devices. **ED-27**.1896-1908 (1980)
60. Zimmerman. J. E.: Sensitivity enhancement of Superconducting Quantum Interference Devices through the use of fractional-turn loops. J. Appl. Phys. **42**. 4483-4487 (1971)
61. Shoenberg. D.: Superconductivity (Cambridge University Press 1962) 30.
62. For a review, see Clarke. J.: Geophysical Applications of SQUIDs. IEEE Trans. Magn. **MAG-19**. 288-294 (1983)
63. De Waal. V. J. and Klapwijk. T. M.: Compact Integrated dc SQUID gradiometer. Appl. Phys. Lett. **41**. 669-671 (1982)
64. Van Nieuwenhuyzen G. J. and de Waal. V. J.: Second order gradiometer and dc SQUID integrated on a planar substrate. Appl. Phy. Lett. **46**. 439-441 (1985)
65. Carelli. P. and Foglietti. V.: A second derivative gradiometer integrated with a dc superconducting interferometer. J. Appl. Phys. **54**. 6065-6067 (1983)
66. Koyangi. M., Kasai. N., Chinore. K., Nakanishi. M. and Kosaka. S.: An integrated dc SQUID gradiometer for biomagnetic application. Proceedings of the Applied Superconductivity Conference August 21-25, 1988 (to be published)
67. Knuutila. J., Kajola. M., Mutikainen. R., Salmi. J.: Integrated planar dc SQUID magnetometers for multichannel neuromagnetic measurements. Proc. ISEC '87 p. 261
68. For reviews, see Romani. G. L., Williamson. S. J. and Kaufman. L.: Biomagnetic instrumentation. Rev. Sci. Instrum. **53**. 1815-1845 (1982); Buchanan. D. S., Paulson. D. and Williamson. S. J.: Instrumentation for clinical applications of neuromagnetism. Adv. Cryo. Eng. (to be published)
69. Knuutila. J.: European Physical Society Workshop "SQUID: State of Art, Perspectives and Applications". Rome, Italy June 22-24, 1988 (unpublished)
70. Barth. D. S., Sutherling. W., Engel. J. Jr. and Beatty J.: Neuromagnetic evidence of spatially distributed sources underlying epileptiform spikes in the human brain. Science **223**. 293-296 (1984)
71. Romani. G. L., Williamson. S. J. and Kaufman. L.: Tonotopic organization of the human auditory cortex. Science **216**. 1339-1340 (1982)
72. Cabrera. B.: First results from a superconductive detector for moving magnetic monopoles. Phys. Rev. Lett. **48**. 1378-1381 (1982)
73. Quantum Design, 11568 Sorrento Valley Road, San Diego, CA 92121.

74. Ketchen. M. B., Kopley. T. and Ling. H.: Minature SQUID susceptometer. Appl Phys. Lett. **44.** 1008-1010 (1984)
75. Awschalom. D. D. and Warnock. J.: Picosecond magnetic spectroscopy with integrated dc SQUIDs. Proceedings of the Applied Superconductivity Conference August 21-25, 1988 (to be published)
76. Clarke. J.: A superconducting galvanometer employing Josephson tunneling. Phil. Mag. **13.** 115-127 (1966)
77. Hilbert. C. and Clarke. J.: DC SQUIDs as radiofrequency amplifiers. J. Low Temp. Phys. **61.** 263-280 (1985)
78. Tesche. C. D. and Clarke. J.: DC SQUID: current noise. J. Low Temp. Phys. **37.** 397-403 (1979)
79. Hilbert. C. and Clarke. J.: Measurements of the dynamic input impedance of a dc SQUID. J. Low Temp. Phys. **61.** 237-262 (1985)
80. Martinis. J. M. and Clarke. J.: Signal and noise theory for the dc SQUID. J. Low Temp. Phys. **61.** 227-236 (1985), and references therein.
81. Koch. R.H., Van Harlingen. D. J. and Clarke. J.: Quantum noise theory for the dc SQUID. Appl. Phys. Lett. **38.** 380-382 (1981)
82. Danilov. V. V., Likharev. K. K. and Zorin. A. B.: Quantum noise in SQUIDs. IEEE Trans. Magn. **MAG-19.** 572-575 (1983)
83. Hilbert. C., Clarke. J., Sleator. T. and Hahn. E. L.: Nuclear quadruple resonance detected at 30MHz with a dc superconducting quantum interference device. Appl. Phys. Lett. **47.** 637-639 (1985). (See references therein for earlier work on NMR with SQUIDS).
84. Fan. N. Q., Heaney. M.B., Clarke. J., Newitt. D., Wald. L. L., Hahn. E. L., Bielecke. A. and Pines. A.: Nuclear magnetic resonance with dc SQUID preamplifiers. Proceedings of the Applied Superconductivity Conference August 21–25 (1988)
85. Sleator. T., Hahn. E. L., Heaney, M.B., Hilbert. C. and Clarke. J.: Nuclear electric quadrupole induction of atomic polarization. Phys. Rev. Lett. **57.** 2756-2759 (1986)
86. Sleator. T., Hahn. E. L., Hilbert, C. and Clarke. J.: Nuclear-spin noise and spontaneous emission. Phys. Rev. B. **36.** 1969-1980 (1987)
87. For an elementary review on gravity waves, see Shapiro. S. L., Stark. R.F. and Teukolsky. S. J.: The search for gravitational waves. Am. Sci. **73.** 248-257 (1985)
88. For a review on gravity-wave antennae, see Michelson. P. F., Price. J. C. and Taber. R. C.: Resonant-mass detectors of gravitational radiation. Science **237.**150-157 (1987)
89. Paik. H. J.: Superconducting tensor gravity gradiometer with SQUID readout. SQUID Applications to Geophysics. Ed. Weinstock H. and Overton. W. C., Jr. (Soc. of Exploration Geophysicists, Tulsa, Oklahoma, 1981) 3-12
90. Mapoles. E.: A superconducting gravity gradiometer. ibid. 153-157
91. Bednorz. J. G. and Muller. K. A.: Possible high T_c superconductivity in the Ba-La-Cu-O system. Z. Phys. **B64.** 189-193 (1986)

92. Koch. R. H., Umbach. C. P., Clark. G. J., Chaudhari. P. and Laibowitz. R. B.: Quantum interference devices made from superconducting oxide thin films. Appl. Phys. Lett. **51.** 200-202 (1987)
93. Zimmerman. J. E., Beall. J. A., Cromar. M. W. and Ono. R. H.: Operation of a Y-Ba-Cu-O rf SQUID at 81K. Appl. Phys. Lett. **51.** 617-618 (1987)
94. Ferrari. M. J., Johnson. M., Wellstood. F. C., Clarke. J., Rosenthal. P. A., Hammond. R. H. and Beasley. M. R.: Magnetic flux noise in thin film rings of $YBa_2Cu_3O_{7-\delta}$. Appl. Phys. Lett. **53.** 695-697 (1988)
95. Shiota. T., Takechi. K., Takai. Y and Hayakawa. H.: An observation of quasiparticle tunneling characteristics in all Y-Ba-Cu-0 thin film tunnel junctions (unpublished)
96. Mankiewich. P. M., Schwartz. D. B., Howard. R. E., Jackel. L. D., Straughn. B. L., Burkhardt. E. G. and Dayem. A. H.: Fabrication and characterization of an $YBa_2Cu_3O_7/Au/YBa_2Cu_3O_7$ S-N-S microbridge. Fifth International Workshop on Future Electron Devices - High Temperature Superconducting Devices. June 2-4, 1988, Miyaki-Zao, Japan. 157-160

LAWRENCE BERKELEY LABORATORY
TECHNICAL INFORMATION DEPARTMENT
1 CYCLOTRON ROAD
BERKELEY, CALIFORNIA 94720